International Journal of Nanomedicine

Dovepress
open access to scientific and medical research

Open Access Full Text Article

REVIEW

# Perfluorocarbons-Based $^{19}F$ Magnetic Resonance Imaging in Biomedicine

This article was published in the following Dove Press journal:
*International Journal of Nanomedicine*

Lina Wu[1,2,*]
Fang Liu[1,3,*]
Shuang Liu[1,2,*]
Xiuan Xu[1,3]
Zhaoxi Liu[1,2]
Xilin Sun[1,2]

[1]NHC and CAMS Key Laboratory of Molecular Probe and Targeted Theranostics, Molecular Imaging Research Center (MIRC), Harbin Medical University, Harbin, Heilongjiang 150028, People's Republic of China; [2]TOF-PET /CT/MR Center, Harbin Medical University, Harbin, Heilongjiang 150028, People's Republic of China; [3]Department of Medical Imaging, Harbin Medical University, Harbin, Heilongjiang 150028, People's Republic of China

*These authors contributed equally to this work



**Abstract:** Fluorine-19 ($^{19}F$) magnetic resonance (MR) molecular imaging is a promising noninvasive and quantitative molecular imaging approach with intensive research due to the high sensitivity and low endogenous background signal of the $^{19}F$ atom in vivo. Perfluorocarbons (PFCs) have been used as blood substitutes since 1970s. More recently, a variety of PFC nanoparticles have been designed for the detection and imaging of physiological and pathological changes. These molecular imaging probes have been developed to label cells, target specific epitopes in tumors, monitor the prognosis and therapy efficacy and quantitate characterization of tumors and changes in tumor microenvironment noninvasively, therefore, significantly improving the prognosis and therapy efficacy. Herein, we discuss the recent development and applications of $^{19}F$ MR techniques with PFC nanoparticles in biomedicine, with particular emphasis on ligand-targeted and quantitative $^{19}F$ MR imaging approaches for tumor detection, oxygenation measurement, smart stimulus response and therapy efficacy monitoring, et al.

**Keywords:** fluorine-19 magnetic resonance imaging, fluorocarbons, nanoparticles, molecular imaging, neoplasms

## Introduction

Fluorine-19 magnetic resonance ($^{19}F$ MR) molecular imaging is a noninvasive tool widely exploited for in vivo applications due to low background signals. Similar to $^{1}H$, $^{19}F$ has a spin of one-half nucleus and no quadrupolar moment, thereby greatly simplifying spectral analysis. The $^{19}F$ nucleus has a high gyromagnetic ratio and a sensitivity of 83%, which is comparable to that of $^{1}H$ and significantly higher than the sensitivity of other typically investigated MR receptive nuclei, such as $^{31}P$, $^{13}C$, and $^{15}N$. The natural abundance of $^{19}F$ is 100%. Endogenous $^{19}F$ is found primarily in bone marrow and teeth as solid fluorides, whereas soft tissues have undetectable $^{19}F$ MR signals.[1] $^{19}F$ is virtually absent from tissues without endogenous background signal.[2] Finally, in addition to its high sensitivity, $^{19}F$ nucleus exhibits a wide range of chemical shifts (>350 ppm) and it is extremely sensitive to relaxation changes, which can provide higher resolution than $^{1}H$ MRI.[3] Thus, administered $^{19}F$-containing compounds have optimal properties for specifically and selectively assessing tissue physiology and pathology in vivo.

Perfluorocarbons (PFCs) are biologically inert, highly stable, non-toxic, non-carcinogenic, non-mutagenic, non-teratogenic compounds that can generate $^{19}F$ signal and they are not metabolized in the human body.[3,4] PFC nanoparticles (NPs) have therefore been extensively used as $^{19}F$ MRI agents in research applications.

Correspondence: Xilin Sun
Molecular Imaging Research Center of Harbin Medical University (MIRC), TOF-PET/CT/MR Center, Harbin Medical University, Harbin, Heilongjiang 150028, People's Republic of China
Fax +86 451-82576509
Email sunxl@ems.hrbmu.edu.cn

submit your manuscript | www.dovepress.com
DovePress
http://doi.org/10.2147/IJN.S255084

The strong C-F bond in PFCs is resistant to cleavage by endogenous enzymes, and the dense, electron-repelling sheath that coats F-chains allows only extremely weak intermolecular interactions.[5] Due to their relatively large size (~250 nm), intravenous administration of PFC NPs is not susceptible to glomerular filtration and is instead removed from the circulation via the reticuloendothelial system and exhalation through respiration.[6,7] Thus, PFCs have excellent biosafety and exhibit no renal toxicity in animals or human, which do not increase kidney burden.[8,9] The frequently used PFCs are perfluorooctyl bromide (PFOB), perfluoro-15-crown-5-ether (PFCE) and perfluoropolyether (PFPE). When compared to iodinated or gadolinium-based contrast agents, PFC NPs are better suited for patients with kidney disease. Research shows that the blood clearance half-life of PFCs ranges from three to 42 hours,[10] and tissue clearance occurs within four (PFOB) to 65 days (perfluorotripropylamine),[11] thereby allowing sufficient time for MR detection. A practical concern persists regarding the application of probes in patients with potentially impaired renal function. Gadolinium agent as a paramagnetic contrast agent for MRI scans is thought to be associated with susceptibility to diseases such as nephrogenic systemic fibrosis.[12–14]

PFCs also have very good respiratory gas- (oxygen and carbon dioxide) carrying capacity and were first proposed as oxygen carriers in 1966.[15] Over the last decade, PFCs have been widely used as oxygen-carrying blood substitutes[16] and for liquid ventilation in respiratory diseases. Besides their low viscosity, liquid PFCs generally have 10–20 times more oxygen solubility than water or blood plasma,[17] and they were shown to maintain oxygen transport and support life for several hours in rats lacking erythrocytes.[18] Thus, PFCs are excellent candidates for protecting tissue from hypoxia and preventing irreversible tissue damage.

PFCs exchange oxygen with the surrounding medium through free diffusion on a millisecond timescale.[19] The oxygen solubility of PFCs varies inversely with temperature, and the amount of oxygen dissolved in any type of PFC increases linearly with oxygen partial pressure ($pO_2$). To measure tissue oxygenation noninvasively, calibration curves can be used to illustrate the relationship between $^{19}F$ concentration and $pO_2$.[20,21] Mechanistically, since $O_2$ is a paramagnetic substance, its partial pressure affects the longitudinal relaxation rate ($R_1$) of PFC in a linear way as follows: $R_1=A+B*pO_2$.[22] Hence, $pO_2$ corresponds to $R_1$ and ultimately to longitudinal relaxation time $T_1$ ($1/R_1$). As a result, by measuring the $^{19}F$ $T_1$ value of different tumor areas (acquiring a $T_1$ map), we can obtain the corresponding $pO_2$.[23–25] Due to these advantages, $^{19}F$ MRI has increasingly being utilized in physiological molecular imaging and therapeutics.[26–28]

The smart stimuli-responsive $^{19}F$ MRI platform using PFC-based nanoprobes with exceptional sensitivity and off/on-switching is a powerful tool for visualizing in vivo enzymatic activity, redox-potential difference, and lower pH values.[29] By combined various stimuli-responsive with theranostic nanoplatforms for sensitive $^{19}F$ MRI of biological and pathological situations, stimuli-responsive nanoparticles will eventually take advantage of specific tumor microenvironmental changes enable early accurate diagnosis and therapeutics. This novel technology is considered to have the potential to clarify the biomolecular networks in animals using the latest molecular imaging techniques.

## $^{19}F$ MRI Techniques

Negligible signal background enables high contrast-to-noise ratios and improved quantification potential in $^{19}F$ MRI. Challenges and future perspectives regarding routine $^{19}F$ imaging for clinical translation of these techniques to patients are specialized coils and hardware for acquisition of $^{19}F$ MR images. To meet these challenges, a variety of $^{19}F$ MR relevant equipment, techniques, and sequences have been developed in recent years. Below we discuss some of the lessons that can be drawn from these advancements in $^{19}F$ MRI technology.

As $^{19}F$ MRI can only trace exogenous fluorinated materials, it is necessary to conduct $^{1}H$ MRI simultaneously to collect anatomical information. Dual-tuned $^{19}F/^{1}H$ radiofrequency (RF) coils for $^{19}F$ MRI have been developed to address this issue and are currently widely used. As the signal-to-noise ratio (SNR) can be maximized by tuning the frequency to either $^{19}F$ or $^{1}H$, this combined approach has significantly improved $^{19}F$ imaging technology.[30,31] Villavalverde et al designed a multi-tuned RF coil based on the high $B_1$ homogeneity of birdcage coils to obtain high-quality images with good uniformity and sensitivity for $^{19}F$.[32] Another study showed that the birdcage coil increased the $B_1$ homogeneity, which allowed estimation of the minimum detectable $^{19}F$ atoms number and $^{19}F$ content of the NP. The minimum detectable PLGA-PFCE concentration was 2.5 mg/mL using the birdcage coil in NP solution phantoms imaging and MRS. In addition, due to the advantage of increased $B_1$ detection sensitivity and field uniformity, the butterfly coil could be used in animal experiments.[33] This dual-tuned $^{19}F/^{1}H$ RF coils have been

successfully applied in preclinical studies. For instance, a $^{19}F/^{1}H$ RF coil improved the $B_1$ field uniformity without reducing sensitivity in MRI of arthritic knee in rabbits.[34] More recently, an eight-channel transceiver $^{19}F/^{1}H$ RF coil employed to locate and quantify administrated fluorinated materials in the knee at 7.0 T showed high sensitivity with an in-plane spatial resolution of 1.5 × 1.5 $mm^2$ and slice thickness of 5 mm, revealing great translation potential to clinical applications. Further technological developments are necessary to promote real-time bioavailability studies and quantification of $^{19}F$-containing medicinal compounds in vivo.[35]

Several MR sequences have been designed to improve SNR and the quantification accuracy of $^{19}F$ MRI.[30] PFCE has been widely investigated as $^{19}F$ MRI contrast agent with a strong single peak resonance spectrum at −91.8 ppm related to $CFCl_3$ without any chemical shift artifact.[36] For $^{19}F$ compounds with unique spectral properties, fast spin echo/rapid acquisition with relaxation enhancement (FSE/RARE) is the most useful sequence.[37] Unlike PFCE, many PFCs have multiple NMR spectral peaks with $^{19}F$ MRI SNR decreased. PFPE has two major chemical shifts at −90.7 and −90.9 ppm used for cellular and molecular MRI.[38] PFOB ($CF_3$-$(CF_2)_6$-$CF_2Br$) is a blood substitute used for $^{19}F$ MRI that exhibits a multi-peak resonance spectrum and complex $^{19}F$ resonances and multiple relaxation conditions with single $^{19}F$ resonance peaks for $CF_2Br$ and $CF_3$ groups and five proximate chemical shift components of the $CF_2$ group.[39,40] The challenge for multispectral compounds with chemical shift artifacts in MRI is that the SNR is reduced if only the signal of a single spectrum is acquired.[38–40] To meet this challenge, Fluorine ultra-fast Turbo Spectroscopic Imaging (F-uTSI)[41] has also been developed to improve SNR without sacrificing sensitivity or increasing scan time. Furthermore, F-uTSI can distinguish between various $^{19}F$ compounds based on chemical shift differences, thereby allowing for "multi-color" imaging. Another approach of meeting this challenge is to adopt a novel pulse sequence, $^{19}F/^{1}H$ 3D-balanced steady-state free precession (bSSFP) to avoid the chemical shift artifacts of PFC with multi-resonance spectra[40] Notably, the bSSFP sequence implemented on a clinical 3 T scanner enabled the detection of PFOB labels with higher sensitivity than traditional techniques. Additionally, by using a $^{19}F$ chemical shift encoding (CSE) approach, Van Heeswijk et al demonstrated that CSE–bSSFP has higher sensitivity than bSSFP-UTE sequences at 3 T.[42] The $T_1$ and $T_2$ relaxation time of three PFC emulsions commonly used in $^{19}F$ MRI were measured at 3 T, including PFOB, PFCE and PFPE at different temperatures. By means of relaxation time for each PFC phantom, the optimized parameters repetition time (TR) and echo train length (ETL) with longitudinal magnetization restoration (LMR) (a −90 "flip-back" pulse) off and on in the turbo spin echo (TSE) pulse sequence and the optimal flip angle for the bSSFP pulse sequence were determined for PFCs.[43] Mastropietro et al proposed a procedure for optimizing the SNR in RARE sequences, which improved sensitivity of $^{19}F$ MR. In this work the optimized RARE parameters (TR, number of echoes, flip back pulse) provided a method of improved SNR according to measured relaxation time ($T_1$, $T_2$) values at 7 T, which might be encountered in vivo and in vitro molecular imaging experiments.[37] Theoretical and experimental comparisons of spoiled-gradient echo (SPGR), RARE, and SSFP pulse sequences were conducted under phantom conditions using $^{19}F$ MRI/MRS at 9.4 T. SSFP yielded the highest mean SNR higher than SPGR and RARE using the homogeneous birdcage coil, whereas there was no additional improvement of $^{19}F$ signals for NP loading concentration beyond 7.5 mg/mL per million cells. In this work, SPGR yielded maximal SNR at long TRs and it is recommended to use it in combination with appropriate flip angle. A detectable limitation of cardiac stem cells was approximately 500k (10k cells/voxel) in fast 2D acquisitions spanning (3–5 min) achieved by the butterfly coil. This method of fast and quantitative in vivo cardiac $^{19}F$ MRI of PFCE-labeled progenitor stem cells using SPGR/SSFP and MRS acquisitions with a butterfly coil provided evidence for preclinical work.[33] In another study, the authors developed a class of novel $^{19}F$ chemical exchange saturation transfer (CEST) imaging probes, which detected multiple metal ions ($Mg^{2+}$, $Ca^{2+}$, $Zn^{2+}$) with a single $^{19}F$ NMR peak from multiple fluorines.[44] These imaging probes exhibited high sensitivity and specificity for detecting metal ions at low concentrations. Schoormans et al introduced an iterative sparse deconvolution method to discriminate different $^{19}F$ compounds and remove chemical shift artifacts arising from multiple resonances at 7 T that was applicable for in vivo imaging.[45] In addition, studies have shown that lanthanide gadolinium ions can increase the relaxation rate of $^{19}F$. Recently, the influence of gadolinium-functionalized PFCE emulsions on $^{19}F$ $R_1$ and $^{19}F$ $R_2$ at different magnetic field strengths was studied. The results indicated that gadolinium-functionalized perfluorocarbon emulsions were suitable for $^{19}F$ MRI at current clinical field strengths (1.5–3.0 T) as gadolinium ions increased the value of $^{19}F$ $R_1$. However, for the emulsions without gadolinium, higher

field strengths (6.3–14 T) are favorable for $^{19}F$ measurements due to the fact that gadolinium does not increases $^{19}F$ $R_1$, but leads to significantly increasing $^{19}F$ $R_2$.[46]

## The Development of PFC Nanoparticles

PFC nanoparticles consist of a PFC core surrounded by a lipid monolayer that can be functionalized with a variety of agents. Different types of PFCs can be used as a core, including perfluorodichlorooctane (PFDCO), perfluorotributylamine (PFTB), perfluorodecalin (PFDC), PFCE, and PFOB. Although PFCE exhibits optimal MRI properties, its long retention time in the human body makes it unsuitable for repetitive clinical applications.[47] On the other hand, a variety of other PFCs, including PFOB, are quickly cleared from the body through exhalation by the lungs. Furthermore, while these compounds may induce chemical shift artifacts when $^{19}F$ images are acquired in a conventional manner due to signal splitting resulting from $^{19}F$ nuclei of different magnetism, this problem can be overcome by advanced detection methods based on fast chemical shift imaging techniques.[48,49] Thus, the $^{19}F$ nucleus in the core of PFC NPs offers many favorable magnetic properties and provides a very high intrinsic signal level.

The surface of nanoparticles can be covalently or non-covalently linked to many types of imaging agents for molecular imaging and therapy, such as florescent material for fluorescence imaging and histology, radionuclides for nuclear imaging, iodine for computed tomography (CT) and paramagnetic metals (Gd, Fe, Mn) for MRI. Positron emission tomography (PET) and single photon emission computed tomography (SPECT) have high sensitivity to detect, visualize, and quantitatively measure molecular targets in the tumor microenvironment. The limitations of PET and SPECT are their poor spatial resolution and relatively high doses of radiation.[50] CT is an imaging technique that offers great advantages such as high spatial and density resolution. However, CT generally has low sensitivity, specificity and temporal resolution visualization of the internal structure of soft tissues.[51] MRI has many advantages such as no ionizing radiation, high-sensitivity, high spatial resolution and high image contrast. MRI is commonly used in anatomic, functional, and molecular imaging.[52] In most MR molecular imaging researches, it is necessary to compare series of pre-/post-contrast images to distinguish superparamagnetic (eg, iron oxide) or paramagnetic metal (eg, gadolinium) contrast from background signals, which can be avoided due to the advantage of negligible $^{19}F$ background signal. Gadolinium agent as a paramagnetic contrast agent for MRI scans is thought to be associated with susceptibility to diseases such as nephrogenic systemic fibrosis and acute complement activation found in clinical trials.[13,53,54] A practical concern persists regarding the application of probes in patients with impaired renal function and potential risk of systemic side effects, which calls for great caution. Superparamagnetic iron oxide (SPIO) particles are very sensitive to cell labeling and have been widely used to label NSCs in preclinical studies.[55] However, due to superparamagnetic bloom artifacts, iron oxide tends to reduce the resolution of soft tissue. Due to the lack of magnetic artifacts of $^{19}F$, these artifacts can be avoided and the details of tissue and cellular boundary images can be preserved.[28] In addition, in vivo cell apoptosis or cell lysis can liberate the iron, which can be engulfed by microglia or macrophages surrounding the transplanted stem cells, leading to false positive signals.[56] More recently, increasing attention has been paid to PFC labeling for MR cell tracking. Furthermore, PFCs can be used as ultrasound molecular imaging agents due to their composition, which allows detection by mechanical waves at clinically relevant imaging frequencies.[57,58] These intrinsic properties of PFCs, therefore, enable the unambiguous detection of exogenously administered PFC NPs and the quantitative monitoring of their biodistribution in vivo with different imaging modalities.[59,60] Finally, the surface of nanoparticles can also be linked with different molecular ligands or drugs for targeted molecular imaging, targeted therapy and other applications (Figure 1).[61]

## The Applications of Perfluorocarbons-Based $^{19}F$ MRI in Oncology

$^{19}F$ MR has many applications in targeted imaging, measurement of tumor oxygenation, monitoring of drug delivery, cell therapy, treatment evaluation, and stimuli-responsive imaging[26,62-70] which will be introduced in detail as follows. Table 1 is a summary of representative studies using $^{19}F$ MR molecular imaging in these applications.

## Ligand-Targeted Tumor Imaging

In recent years, targeted paramagnetic PFC NPs have been widely used in $^{19}F$ MRI for the recognition of pathological biomarkers, for the detection of changes in expression

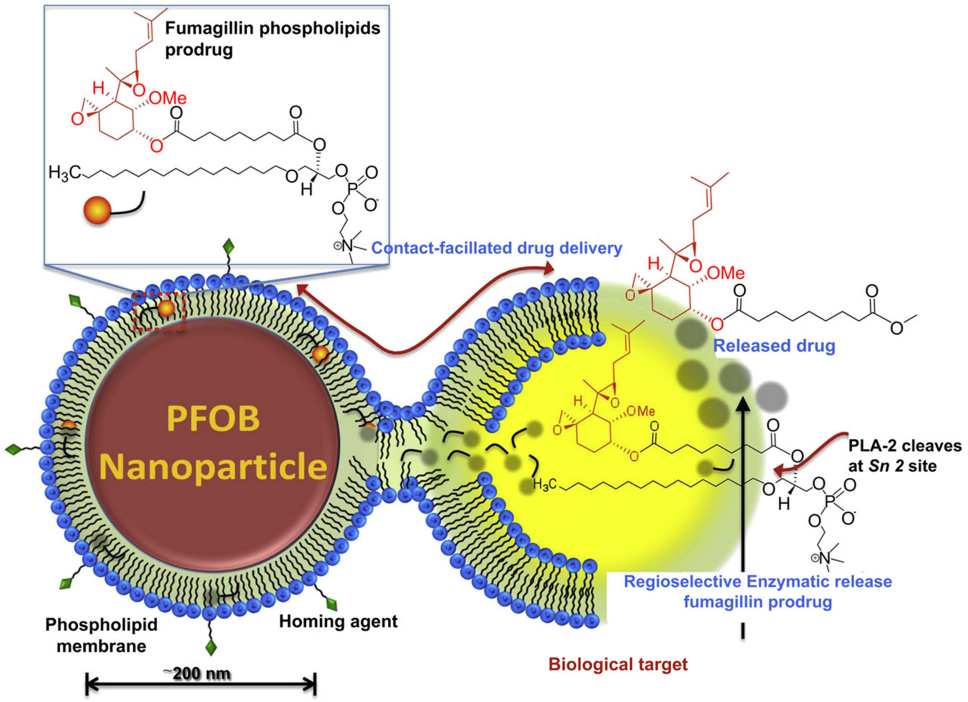


**Figure 1** Schematic representation of the contact-facilitated drug delivery mechanism. Reprinted with permission from Zhou H-F, Yan H, Senpan A et al Suppression of inflammation in a mouse model of rheumatoid arthritis using targeted lipase-labile fumagillin prodrug nanoparticles. *Biomaterials*. 2012;33(33):8632–8640.Copyright © 2012 Elsevier Ltd.[61]

levels due to disease development, in therapeutic interventions, or in the monitoring of disease recurrence. A variety of $^{19}$F-based imaging tracers have been introduced, including micelles,[71] liposomes,[72] and emulsions.[73] The physicochemical properties of PFC NPs, combined with their high surface area, which can incorporate 50 to 500 targeting ligands, allow the detection of sparse concentrations of cell surface biomarkers. Furthermore, the incorporation of large amounts of paramagnetic materials into the nanoparticles was shown to increase the contrast of molecular epitopes occurring in very small quantities in vivo.[74,75]

PFC NPs or nanoemulsions covered with tumor-specific ligands have been extensively explored in noninvasive imaging and drug delivery. Most early research on MRI using targeted PFC materials was focused on $^{1}$H MRI. For example, in a study with Vx-2 rabbit tumor models, the $^{1}$H MR signal intensity increased by 56% in the $\alpha_v\beta_3$-integrin-targeted PFC NPs injected group, and this signal was significantly reduced by competitive blocking with $\alpha_v\beta_3$-integrin nonparamagnetic nanoparticles.[76] Diou et al modified the capsule morphology of PFOB nanocapsules for detecting tumors with $^{19}$F MRI, and were able to distinguish between passive and active targeting after decorating the particles with 600–950 integrin-binding RGDS peptide.[77] In another study, the dependence of neovascular molecular MRI on the relaxation time ($R_1$) of $\alpha_v\beta_3$-integrin-targeted paramagnetic PFC NPs was determined. The authors traced the temporal-spatial consistency of angiogenesis assessments in a rabbit Vx2 tumor model and compared the neovascular contrast enhancement obtained with $\alpha_v\beta_3$-integrin-targeted Gd-DOTA-PE and $\alpha_v\beta_3$-integrin-targeted Gd-DTPA-BOA nanoparticles.[78] MR neovascular contrast maps of Vx2 tumors at various time points after implantation revealed that surface enhancement is progressive and temporally consistent.

Despite the recent advances in $^{19}$FMR targeted imaging with PFC NPs, most studies focus on $\alpha_v\beta_3$-integrin,[77,79,80] folate receptor (FR)[81–85] and vascular endothelial growth factor receptor 2 (VEGFR2)[86,87] as molecular targets to detect tumor angiogenesis, proliferation and certain cardiovascular disease (Figure 2). $^{19}$F MRI of brain tumor angiogenesis with integrin-targeted PFC NPs in mice carrying U87 glioblastoma achieved a 50% increase in signal in the targeted group.[79] Waters et al used $^{19}$F diffusion weighted MR spectroscopy (DWS) at 11.7 T to detect angiogenesis in vivo with $\alpha_v\beta_3$-integrin-targeted PFC NPs in an epidermal squamous carcinomas mouse model (K14-HPV16). Progressive decay of the $^{19}$F signal with increased diffusion weighting at b-values below 1500 s/mm$^2$ was observed in both K14-HPV16 and

**Table 1** Applications of $^{19}F$ MR in Molecular Imaging

| | Year | Type of PFC | Imaging Purposes | Models | Ref |
|---|---|---|---|---|---|
| Cell tracking | 2005 | perfluoropolyether | cell tracking | dendritic cells | [185] |
| | 2007 | PFOB and PFCE | cell tracking | stem/progenitor cells | [138] |
| | 2008 | PFCE | cell tracking | stem cells | [187] |
| | 2010 | PFPE | cell tracking | antigen-specific T cells | [115] |
| | 2014, 2015 | PFPE | stroke-damaged brain imaging | human neural stem cells (hNSCs) | [55,136] |
| | 2016 | PFPE and PFOB | cellular imaging | glioma cells | [188] |
| | 2019 | PFCE | cell tracking and therapy | dendritic cells | [189] |
| | 2019 | PFCE | cardiac quantitative imaging | progenitor stem cells and macrophages | [33] |
| Non-oncological applications | 1989 | perfluorotributylamine and perfluorodecalin | anatomic distribution | mice | [190] |
| | 1992 | perfluorotripropylamine | organ biodistribution | rats | [191] |
| | 2004 | PFCE | molecular imaging of fibrin-targeted | ex vivo human samples | [192] |
| | 2009 | perfluorooctylbromide | tissue factor-targeted drug delivery | vascular smooth muscle cells | [193] |
| | 2011 | PFOB | inflammation quantitative imaging | rats | [194] |
| | 2012 | PFOB | $\alpha_v\beta_3$ integrin targeted | rabbits | [195] |
| | 2013 | PFCE | intravascular oxygen tension evaluation | mice | [196] |
| Oncological applications | 1987 | perfluorotributylamine | anti-CEA antibody labeled $^{19}F$ imaging | mice | [197] |
| | 1992 | PFOB | vascular perfusion volume evaluation | mice | [198] |
| | 1993 | perfluorotributylamine | oxygen tension and temperature measurement | mice and rats | [199] |
| | 1996 | PFOB and perfluoro-15-crown-5 | blood volume measurement | mice | [200] |
| | 2016, 2018 | PFOB | folate receptor-targeted imaging | mice | [81,201] |
| | 2017 | PFOB | angiopep-2 peptide targeted therapy | mice | [202] |
| | 2017 | PFOB | hyaluronic acid targeted therapy | mice | [203] |
| | 2018 | PFOB | orthotopic cancer imaging | rabbits | [204] |

**Abbreviations:** PFC, perfluorocarbon; PFOB, perfluorooctyl bromide; PFCE, perfluoro-15-crown-5-ether; PEPE, perfluoropolyether.

control mice, showing that background $^{19}F$ signal from unbound nanoparticles is suppressed in the blood. Whereas K14-HPV16 mice maintained a stationary $^{19}F$ signal at high b-values in the ears, indicating profuse binding of PFC NPs to angiogenesis, the $^{19}F$ signal in controls decayed completely at high b values (>1500 s/mm$^2$) due to absence of binding. These results show that in vivo $^{19}F$ DWS is useful for specifically detecting bound PFC NPs by selectively suppressing background $^{19}F$ signal from unbound nanoparticles flowing in blood.[88] Angiogenesis-targeted PFOB nanoparticles in a rabbit Vx2 tumor model revealed heterogeneous areas of neovasculature at the tumor rim, as expected, whereas the resultant $^{19}F$ signal overlaid with the $^{1}H$ MR signal clearly elucidated the anatomical colocalization of the heterogeneous distribution of the nanoparticles (Figure 2).[89] Bae et al synthesized folate-targeting PFC/rhodamine nanoemulsions for MR and optical imaging and showed that the nanoprobe was successfully delivered into FR-positive tumor xenograft models of nasopharyngeal carcinoma, with significantly enhanced $^{19}F$ signal intensities in the tumor region in MR and fluorescence imaging. Folate-PFC/rhodamine nanoprobes therefore have excellent tumor-targeting ability and stability in vivo.[90]

Although EGFR is highly expressed in a variety of malignant tumor cells, including non-small cell lung cancer

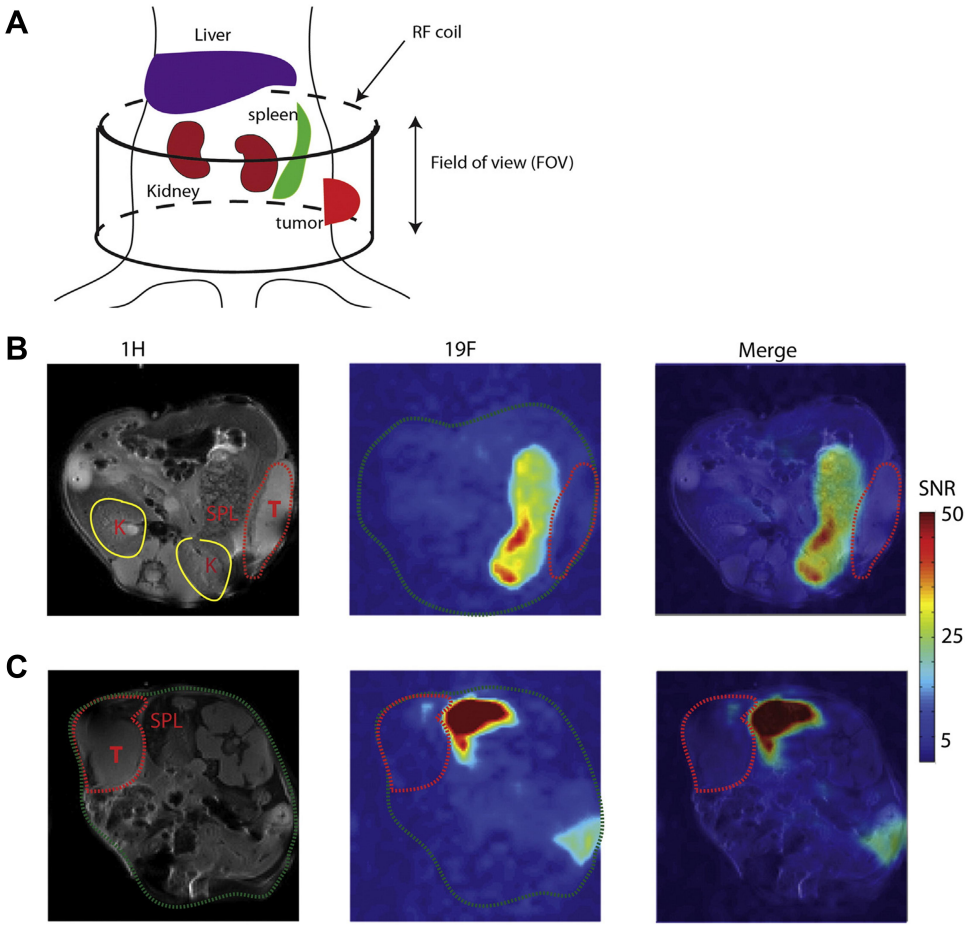


**Figure 2** (**A**) Illustration shows the position of RF coil in the MRI scan. In vivo MRI of mice administered with PLGA-PEG PFOB/ICG (**B**) or PLGA-PEG-folate PFOB/ICG (**C**) $^{1}$H: anatomical images, $^{19}$F: $^{19}$F MRI SNR map, merge: $^{1}$H and $^{19}$F merged, T: tumor region, SPL: spleen, K: kidney.
**Notes:** Reprinted with permission from Vu-Quang H, Vinding MS, Nielsen T, *et al*. Theranostic tumor targeted nanoparticles combining drug delivery with dual near infrared and $^{19}$F magnetic resonance imaging modalities. *Nanomedicine*. 2016;12(7):1873–1884. Copyright © 2016 Published by Elsevier Inc.[81]

(NSCLC),[91] head and neck cancer,[92] and ovarian cancer,[93] fewer studies have explored the potential of targeting EGFR in $^{19}$F MRI to detect tumors cells. EGFR is an important transduction signal pathway involved in tumor cell growth, proliferation, angiogenesis, adhesion, invasion, metastasis and apoptosis. Thus, the non-invasive detection of EGFR in tumors is critical for early diagnosis and successful cancer treatment. For instance, PFC NPs carrying oxygen and the EGFR tyrosine kinase inhibitor (EGFR-TKI) erlotinib showed an important anti-tumor effect, revealing that PFC NP therapy targeting EGFR is a promising therapeutic strategy.[94] Thus, EGFR-targeted PFC NPs that can simultaneously assess $pO_2$ show great potential for tumor detection, monitoring and therapy.

## Measurement of Tumor Oxygenation

Regional hypoxia is common in solid tumors due to their poorly organized vasculature network and high oxygen demands of proliferating tumor cells. Growing evidence shows that hypoxia promotes tumor angiogenesis, recurrence, progression, metastasis,[95] and sensitivity to radiotherapy. Currently, a wide variety of techniques are available to measure tumor oxygenation.[96] Methods to measure absolute $pO_2$ include polarographic oxygen electrodes and fluorescence quenching fiberoptic probes, as well as electron paramagnetic resonance oximetry and $^{19}$F relaxometry.[95] However, many of these approaches are highly invasive or cannot be applied to longitudinal studies of oxygen dynamics.

$^{19}$F MRI can be used to assess $pO_2$ in tissues quantitatively, which greatly increases the accuracy of tumor detection. As PFC has a high capacity of dissolving $O_2$, when a PFC emulsion injected intravenously reaches tumor tissues the $O_2$ rapidly interchanges between PFC and the surrounding tissue by free diffusion, until equilibrium is achieved.[25,97] Thus, the $pO_2$ of different tumor areas can be assessed by measuring the $pO_2$ of the PFC in

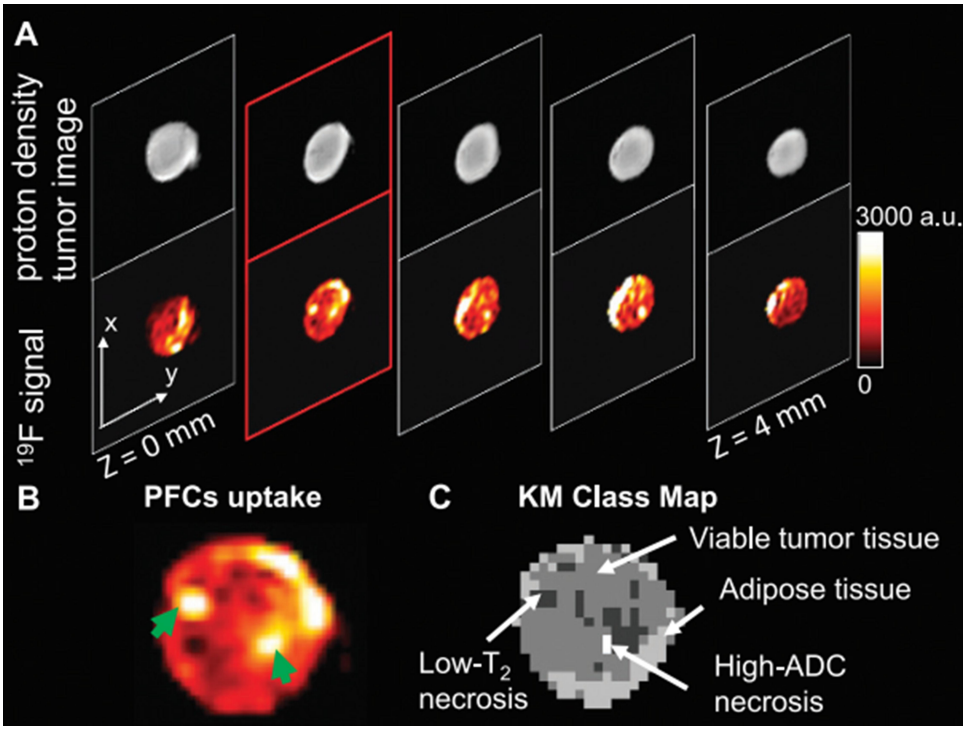


**Figure 3** Anatomic images of PFC uptake in an HM-7 xenograft tumor at 9.4 T with a $^{1}$H/$^{19}$F 10-mm surface coil.
**Notes:** (**A**) The $^{19}$F density images acquired in the same anatomic locations with $^{1}$H density images reveal variable, albeit adequate PFC uptake. (**B**) A sample image of PFC uptake from the second slice in A is highlighted in red. (**C**) The corresponding KM class map for the slice in B revealed that strong uptake of PFCs occurred in some areas of viable tumor, some areas of adipose tissue, and the low-$T_2$ necrosis class. Reproduced with permission from Shi Y, Oeh J, Easthamanderson J et al Mapping in vivo tumor oxygenation within viable tumor by $^{19}$F-MRI and multispectral analysis. Neoplasia. 2013;15(11):1241–1250. Copyright © 2013 Neoplasia Press, Inc.[111]

the corresponding tissue.[22] For given magnetic field and temperature, the dissolved $O_2$ has paramagnetic properties that affect the relaxation rate ($R_1$) of PFC in linear proportion to $pO_2$.[98] Thus, many studies use $^{19}$F MR relaxometry based on the linear relationship between the $R_1$ of $^{19}$F-spins in PFCs and $pO_2$ to noninvasively measure tissue oxygenation locally or globally.[99–101]

The noninvasive measurement of $pO_2$ in tissues plays a key role in the treatment of tumors. Currently, the treatment efficacy of conventional radiotherapy and chemotherapy for malignant tumors is not satisfactory, largely because prevalent hypoxic areas in the tumor may cause resistance to these treatments. Thus, to some extent the noninvasive detection of $pO_2$ in tumor tissue can play a guiding role in cancer treatment. Furthermore, oxygen content in tumors may be improved, ultimately leading to a beneficial therapeutic effect. Specifically, as PFC has a high capacity to dissolve and carry oxygen to tumors, it can change local $pO_2$ and assist in treatment. In addition, $^{19}$F MRI can reveal changes in $pO_2$ in tumors before and after application of PFC, thereby allowing the monitoring of its therapeutic effects. Thus, the noninvasive quantification of tumor oxygenation not only provides unique insights into tumor biology and pathobiology, but it may also be important for developing new treatments[102] and monitoring tumor response.[103] It is critical to develop dynamic methods for direct oxygen mapping.

Quantitative $^{19}$F MRI is the most extensively explored imaging method for in vivo mapping of tumor oxygenation due to the excellent oxygen-carrying capacities of PFCs and fast gas-exchange rate with surrounding tissues.[97] Hypoxia-responsive $^{19}$F MRI probes with improved redox properties and biocompatibility have been synthesized to detect hypoxia.[104] Furthermore, as mentioned above, the $^{19}$F NMR spin-lattice relaxation rates $R_1$ of PFC emulsions are highly sensitive to $pO_2$.[105] PFCs can be administered intravenously or directly by intratumoral injection of PFC droplets or emulsions. Finally, tumor hypoxia measured with PFC NPs strongly correlates with tumor size,[106–108] and generally larger tumors possess a lower baseline $pO_2$.[81]

The method of intravenous administration may affect the relative spatial distribution of PFC and produce the accumulation of PFC in other tissues, such as the liver and spleen. In addition, intravenous administration often results in lower tissue concentrations of PFC in areas of

poor vascularization. SNR of these areas is too low to measure $pO_2$ accurately. This technique may bias $pO_2$ measurements toward regions close to the blood vessels and areas with higher perfusion and oxygenation, resulting in erroneous overestimation of tumor $pO_2$, which may be a major challenge for clinical translation (Figure 3).[109–111] Fast $^{19}F$ MRI techniques, such as fluorocarbon relaxometry using echo planar imaging, have been developed for dynamic mapping of tumor $pO_2$ distributions within tumors, with 5–10% of tumor volume being observed with typical signal.[112] $^{19}F$ MR dynamic monitoring of tumor oxygenation with intratumoral-injected hexafluorobenzene is an important tool to characterize tumor acute hypoxia.[113,114] Kadayakkara et al successfully measured intracellular $pO_2$ ex vivo in labeled glioma cells using $^{19}F$ MRI. This $pO_2$ measurement procedure only required 8 min and had a precision of 1–3 torr at 30–100 individual regions across a tumor. In addition, the authors showed that cellular oximetry may be used to monitor the efficacy of chemotherapy in CNS glioma.[115]

In summary, $^{19}F$ MRI-based $pO_2$ mapping with PFCs has been successfully performed in animal models using clinically achievable field strengths (<7 T). The future translation of this technique to humans will significantly advance tumor-targeted noninvasive imaging and ultimately improve prognosis and the prediction of patient response to therapy.

## Cell Tracking

Cell tracking permits the visualization and monitoring of cells labeled noninvasively ex vivo or in situ. Recently, $^{19}F$ MRI has been utilized to monitor and quantify the in vivo biodistribution of immune cells labeled ex vivo with PFC NPs.[60,70,116-119] For in vivo imaging, systematic intravenous injection of relatively large volumes of PFC NPs is performed. PFC NPs are engulfed by various subgroups of leukocytes, predominantly monocytes, macrophages, neutrophils, and dendritic cells (DCs), as part of their natural clearance from the body. $^{19}F$-labeled leukocytes, often resident in the spleen, are recruited by cytokines into inflamed areas and can be monitored via $^{19}F$ MRI. This method has been used in different animal models to visualize myocardial infarction and myocarditis,[120,121] pneumonia,[122] atherosclerosis,[123] arthritis,[124] and tumors infiltrated by macrophages.[125–127]

Constantinides et al demonstrated the ability to in vivo track and detect intra-cardiac injections of PFCE-NP-labeled cardiac progenitor stem cells (CPCs) at 9.4 T PFCE-NP label uptake in CPCs are maximized for murine cardiac CPC $^{19}F$ MRI by employing DNA transfection (FuGENE), which could be translatable to the clinic.[128] In addition, they further used Medium-chain length polyhydroxyalkanoates (MCL-PHAs)/polycaprolactone (PCL) blend scaffolds for controlled release of seeded CPCs in cardiac tissue engineering (CTE) applications. They found that PFCE-labeled CPCs $^{19}F$ MRI signal and visibility could be improved in the double-layered scaffolds.[126] Ramos et al investigated the time course of inflammatory cell recruitment using PFPE and gadolinium-based elastin-specific magnetic resonance contrast agent (Gd-ESMA) in vivo in a murine model after post-myocardial infarction (MI) using a 3 T clinical scanner. In this study, they noninvasively assess and quantify cardiac inflammation extracellular matrix (ECM) remodeling of the myocardium at the molecular level.[129] Another study demonstrated the ability to use $^{19}F$-MRI cell tracking to detect, quantify and track human mesenchymal stem cells (hMSC) labeled with Cell Sense in vivo on 3D images at 9.4 T after grafting. In this study they showed strong linear between the number of labeled cells implanted and the real cell number by $^{19}F$-MRI.[130]

Noninvasive monitoring of administered T cells labeled ex vivo could potentially allow the prediction of patient response to immunotherapy. Furthermore, as T cells can recognize tumor antigens and migrate to and infiltrate tumor tissue,[131] they may also be used as a probe to detect tumor cells at metastatic sites. Gonzales et al labeled splenocytes and ovalbumin (OVA)-specific T cells with PFCs in vitro for $^{19}F$-MRS/MRI detection in liver, lung, and spleen in control and B16 OVA melanoma-bearing mice. The authors concluded that non-dividing $^{19}F$-labeled cells appear most promising for $^{19}F$ MRS/MRI-based cell tracking.[132] Clinical $^{19}F$ MRI cell tracking using PFPE nanoparticle labeling was conducted in patients with colorectal adenocarcinoma to detect autologous immunotherapeutic mature dendritic cells.[117] PFPE was incorporated into non-phagocytic cells without adjunctive cationic lipids or causing changes in cellular phenotype. Notably, only viable cells were labeled with PFPE. This is therefore a promising technique for detecting tumor cells in vivo and, importantly, for monitoring adopted cell transfer cancer therapies noninvasively. Furthermore, a recent study using $^{19}F$ MRI to detect tumor-associated macrophages (TAM)[49] revealed that $^{19}F$-based cell tracking approaches represent TAM density more reliably and provide more information than other

methods.[129] The commercially available PFC-based agents include Cell Sense and V-Sense (Celsense, Inc., Pittsburgh, USA) used for cell tracking in MRI. These types of labelling agents include fluorinated emulsions (CS-1000 and VS-1000H) and other fluorescently tagged formulations (CS-ATM DM Red, Green, NIR) for ex vivo and in situ cell labels.[133,134] A recent study showed that it is possible to effectively label hMSCs with cell sense without affecting cell viability, function or differentiation. The bSSFP sequence was used to detect and quantify the signal of Cell Sense-labeled hMSC cells in vitro and in -intramuscular implantation.[135] Tennstaedt et al also showed that transgenic hNSCs with stable expression of reporter genes Luciferase and GFP were further to be labeled with PFPE. This strategy provided a new multimodal imaging approach for in vivo application of transgenic hNSCs in deep brain implantation studies.[55] Neural stem cells (NSCs) have labelled with CS-1000 or CS green and luciferase expression were implanted in the striatum. This study investigated the viability of NSCs in stroke animals that underwent focal cerebral ischemia compared to healthy one using $^{19}$F MRI in combination with bioluminescence imaging.[136]

Fink et al reported $^{19}$F MRI as a non-invasive imaging method capable of detecting and quantifying PFC-labeled DC migration at both 9.4 T and 3 T and suitable for therapeutic cell tracking in tumor-bearing mouse models. In addition, viability, phenotype, and function of more than 90% of DC labeled with PFC remained unchanged.[137] A detection limit of,10,000 cells for PFOB-labeled (bearing 17 fluorine atoms) cells with $^{19}$F MRS (11.7 T) was found in vitro. For in situ imaging at 1.5 T, the injection of 4 million PFCE-labeled stem cells could be detected a strong fluorine signal within 7 min. PFCE contains 20 equivalent fluorine atoms per molecule that allow a detection limit of approximately 2000 PFCE-labeled cells with $^{19}$F MRS and approximately 6000 PFCE-labeled cells/voxel in vitro with $^{19}$F MRI (11.7 T) within 7 min.[138] Boehmsturm et al found that human neural stem cells (hNSCs) can be labeled with a PFC marker as well as detected and measured the number of transplanted stem cells in vitro and in vivo after transplantation in the striatum of mouse brain. Related measurements suggested a detection limit of 1000 PFPE-labeled (containing more than 40 fluorine atoms per molecule) cells/voxel was found in vitro and 10,000 cells/voxel to generate significant SNR in vivo at 11.7 T.[118]

Isoflurane (ISO) is a fluorinated anesthetic commonly used in animal models owing to its minimal cardiodepressive effects.[139] Constantinides et al reported that isoflurane exhibited two resonances of $^{19}$F atoms correspond to the -$CF_3$ and -$OCHF_2$ moieties with chemical shifts of −4 and −10.3 ppm with respect to the trifluoroacetic acid (TFA) resonance at 0 ppm in the NMR spectrum. These peaks are close to the resonances of PFCs with chemical shift range of −50–86 ppm relative to TFA due to potential spectral overlaps. PFCE-labeled cells exhibited a single spectral peak at −16.25 ppm with respect to TFA in vitro that did not overlap with the ISO resonances. ISO effects on PFCE labels are minimal but may have more prominent effects on PFPE or PFOB.[140,141] A study investigated that an efficient imaging technique will also minimize any potential $^{19}$F signal from the use of inhalational isoflurane anesthesia by using helpful image acquisition parameters. They use narrow 1.5 kHz sinc excitation pulse and shorter TE (eg, TE 1.8 ms), which is simultaneously beneficial for detecting signals from both cells and isoflurane.[130] Thus, the use of ISO still has a primary choice for $^{1}$H and multinuclear imaging studies.

The advantage of $^{19}$F MRI in ex vivo-labeled cell tracking is the complete absence of background signal due to the negligible amount of $^{19}$F in the body. Finally, $^{19}$F MRI has strong potential as an accurate quantification method of local cell numbers.

## Drug Delivery and Therapy Efficacy Monitoring

The high $^{19}$F signal of PFCs allows the noninvasive quantification of ligand-bound PFC NPs, which in turn enables clinicians to confirm tissue drug concentrations during targeted therapy. Nanoparticles can be engineered to carry highly potent drugs and deliver them to specific cell populations displaying biosignatures of particular diseases. For instance, Rapoport et al recently reported novel drug-loaded PFC emulsions stabilized by biodegradable amphiphilic block copolymers.[142–145] PFC emulsions can deliver lipophilic therapeutic agents to solid tumors while simultaneously allowing the monitoring of their in vivo biodistribution. Furthermore, anti-angiogenic agents have played a critical role in the treatment of various types of tumor, including solid tumors.[146,147] $\alpha_v\beta_3$-integrin-targeted fumagillin-loaded nanoparticles suppressed neovasculature and inhibited tumor growth in Vx2 adenocarcinoma models without causing organ toxicity or neurocognitive dysfunction.[148] Notably, therapeutic efficacy for these targeted nanoparticles occurred

at systemic doses about 1000-fold lower than those used in previous animal studies, and 60-fold lower than doses tested clinically for related anti-angiogenic compounds (TNP-470).

$^{19}$F MRI has been used as a platform for guiding high-intensity focused ultrasound (HIFU) tumor ablation by quantitatively tracking the accumulation of PFC nanoemulsions (PFCNE).[149] PFCNE accumulation in the tumor periphery was clearly visible and quantifiable, and was confirmed by fluorescence imaging. Encapsulated PFCs can also be used for image-guided HIFU ablation and indeed, it was shown that PFOB can increase HIFU effectiveness.[150] Docetaxel-loaded PFCE nanodroplets (Doc-nd) developed by Gupta et al favored passive accumulation into most tumors due to their small particle size, thereby potentially increasing localized drug concentration.[151] A high encapsulation efficiency of 93.70% was obtained for Doc-nd, and Docetaxel was released in a three-stage release kinetic pattern, with an initial release of 30% within an hour, followed by a 50% release within 12 hours and a 85% release after three days. This study suggests that Doc-nd combined with MR-guided focused ultrasound has great potential for treating prostate cancer.

Immune cell therapy has become an effective method to treat cancer, and NK cells are among the immune cell types used in this treatment.[152] Recently, Bouchlaka et al had labelled human NK cells with PFC and injected them into tumors.[153] Strikingly, the PFC remained in the tumor up to 8 days after injections, as detected by $^{19}$F MRI. Another study on the application of poly(D,L-lactic-co-glycolic acid) (PLGA) entrapping PFCE and indocyanine green (ICG) focused on $^{19}$F MRI, fluorescence imaging and photoacoustic imaging (PAI), which could be used for detection of metastasis in melanoma patients.[154] This work showed the potential of labeled primary human dendritic cells for cell imaging and lymph node detection with PAI and $^{19}$F MRI.[155] Thus, $^{19}$F MRI is an effective method of monitoring immune cell therapy.

## Stimuli-Responsive $^{19}$F MRI

Recently, the development of smart stimuli-responsive nanoparticles characterized by the off/on regulation of $^{19}$F MRI signals has attracted much attention. These $^{19}$F MRI probes are suitable for noninvasive visualization of enzymatic activity, redox-potential difference, and pH.[104,156,157] PFC NPs have been used to monitor specific biological events in living animals with an off/on $^{19}$F MRI switch for detecting enzymatic activity based on the paramagnetic relaxation enhancement effect (PRE) for spin-spin relaxation ($T_2$) of $^{19}$F MRI signal without endogenous background signals.[158] Because of the large electron spin quantum number, $Gd^{3+}$ and $Mn^{2+}$ have a very strong PRE effect on the MRI signal of $^{19}$F. The shielded $^{19}$F MRI signal of PFC by the adjacent $Gd^{3+}$ was triggered to turn on because of the cleavage of enzyme (Figure 4).[159] Guo et al reported PFCE NP for in vivo turn-on $^{19}$F MRI sensing the activity of phospholipase A2 (PLA2) with low background (Figure 5).[160] In addition, this off/on $^{19}$F MRI switching strategy broadly applied to detect the activity of various enzymes, such as caspase-1, caspase-3/-7, and matrix metalloproteinases.[29,161,162]

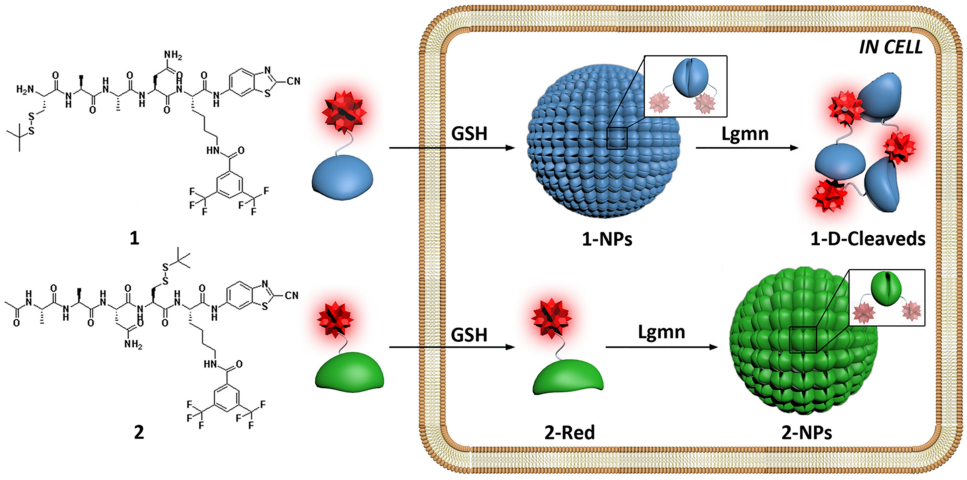


**Figure 4** Schematic illustration of intracellular GSH-controlled self-assembly followed by Lgmn-controlled disassembly of 1-NPs, showing respective "off" and "on" $^{19}$F NMR signals for Lgmn detection, and Lgmn-controlled self-assembly of 2-NPs results in $^{19}$F NMR signals "off" inside cells. Reprinted with permission from Yuan Y, Ge S, Sun H, et al. Intracellular self-assembly and disassemblyof 19F nanoparticles confer respective "off" and "on" 19FNMR/MRI signals for legumain activity detection in zebrafish. ACSNano. 2015;9(5):5117–5124. Copyright © 2015, American Chemical Society.[159]

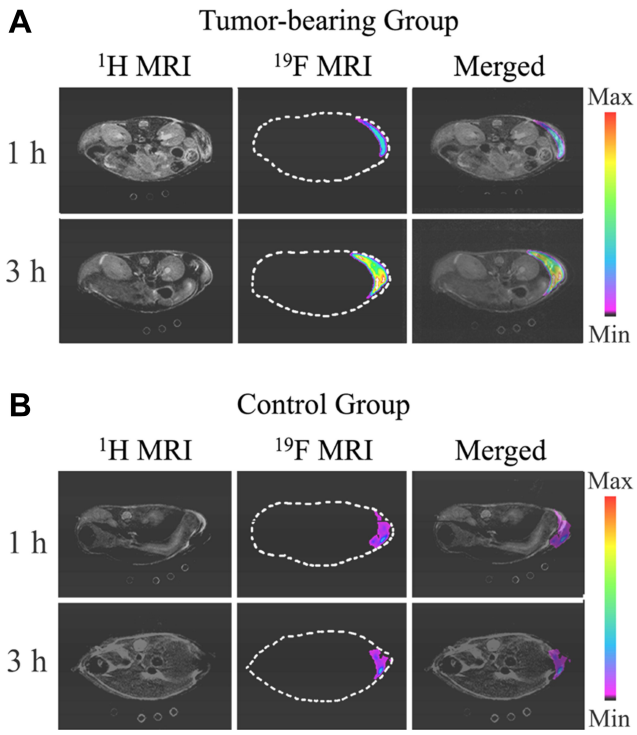


**Figure 5** In vivo $^{1}$H, $^{19}$F MRI, and merged images of $^{1}$H and $^{19}$F MRI for (**A**) a tumor-bearing mouse and (**B**) a healthy mouse. Adapted from Guo C, Zhang Y, Li Y et al $^{19}$F MRI nanoprobes for the turn-on detection of phospholipase A2 with a low background. *Anal. Chem.* 2019;91(13):8147–8153. Copyright © 2019 American Chemical Society.[160]

Reducing microenvironment plays an important role in biological processes and abnormal redox reactions. Nakamura et al reported an activatable reduction-responsive PFC-encapsulated NP, FLAME-SS-$Gd^{3+}$ (FSG), that can be used for in vivo $^{19}$F MRI.[163] In the presence of the disulfide of FSG, $Gd^{3+}$ was removed from the reduced FSG surface and the subsequent $^{19}$F NMR/MRI signal intensity of the encapsulated PFCE would be increased. The highly sensitive detection and visualization of reducing microenvironment in vivo could provide effective information about biological functions for monitoring the process of disease and evaluating the effect of therapy.[164–166]

Solid tumors have a slightly lower extracellular pH (pHe) than the normal tissue environment due to fast growing tumor cells, which causes increased glycolysis and accumulation of lactic acid as an intrinsic feature of the tumor phenotype.[167,168] Acidic environments with low pH have been used as a trigger for environment-responsive tumor imaging. These highly sensitive pH-responsive $^{19}$F probes are a potential smart platform for precise and specific detection of tumors.[169,170] Zhang et al developed a novel pH responsive $^{19}$F probes, Mn-LDH@PFPE NP, which is activated specifically within the acidic tumor environment.[171] The $^{19}$F MRI signals from NPs are at physiological pH 7.4, but activated at extracellular pH 6.5. In vivo experiments reveal that an intense $^{19}$F MR signal can be detected in the tumor after injection of NPs. pH activated NPs are a potential smart $^{19}$F MRI agent for recognizing subtle pH differences.[172,173]

# Perfluorocarbons-Based $^{19}$F MRI in Non-Oncological Applications

## Molecular Imaging of Thrombus

The use of $^{19}$F MRI for thrombus diagnosis dates back more than a decade. Thrombus is rich in molecular epitopes for targeting, in particular fibrin, thrombin, and in some instances, platelets. More recently, noninvasive detection of deep venous thrombi and subsequent pulmonary thromboembolism using $^{19}$F MRI and α2-antiplasmin peptide (α2AP)–targeted PFC nanoemulsions were reported.[174] In this study, developing thrombi with a diameter <0.8 mm could be visualized unequivocally in vivo as hot spots in the murine inferior vena cava, via the simultaneous acquisition of anatomic matching $^{1}$H and $^{19}$F MR images at 9.4 T, with excellent signal-to-noise and contrast-to-noise ratios (71±22 and 17±5, respectively). Furthermore, α2AP-PFCs were successfully utilized in the diagnosis of experimentally induced pulmonary thromboembolism.

## $^{19}$F Angiogenesis Imaging

Angiogenesis is a critical process in some tissues, including the endometrium, bone growth plates, and wound healing, but also in pathologies such as rheumatoid arthritis, atherosclerosis, and asthma. In addition, abnormal angiogenesis is one of the hallmarks of cancer. High-resolution $^{19}$F imaging of angiogenesis was first used to detect and quantify neovasculature in a rabbit model of aortic valve disease with $\alpha_v\beta_3$-PFC nanoparticles.[175] Notably, the valves of rabbits treated with targeted PFC NPs had 220% more fluorine signal than those of rabbits treated with untargeted PFC NPs ($p < 0.001$). Pretreatment of the rabbits with targeted oil-based nonsignaling nanoparticles reduced the fluorine signal by 42% due to competitive inhibition. Finally, integrin-targeted PFC NPs specifically detected early angiogenesis in sclerotic aortic valves of cholesterol fed rabbits.

## $^{19}$F MR Imaging in the Lung

Whereas $^{19}$F MRI with PFC NPs has been widely used to study a variety of diseases, the application of $^{1}$H MRI in the lung is limited, mainly due to the intrinsically low proton density, respiratory motion, and magnetic susceptibility artifacts of the air-tissue interfaces. Early neovascular expansion in the lungs is very difficult to assess noninvasively in patients, in particular quantitatively. However, the addition of an exogenous contrast agent makes the visualization of pulmonary structure and function possible. PFC materials have the distinct advantages of high $^{19}$F MRI sensitivity,[69] excellent oxygen-carrying capacities, lower cost, and the lack of a $^{19}$F background signal within the body. Numerous studies have successfully used $^{19}$F MR with PFC materials to image morphology and function in animal and human lungs.[176–178] For instance, Schmieder et al conducted simultaneous $^{19}$F/$^{1}$H MR molecular imaging with $\alpha_v\beta_3$-targeted PFC NPs to quantitatively assess neovascular expansion of the bronchial arteries following pulmonary artery ligation.[178] The authors demonstrated that $^{19}$F/$^{1}$H MR molecular imaging with $\alpha_v\beta_3$-targeted PFC NPs provides a means to assess the extent of systemic neovascularization in the lung. $^{19}$F MRI may also be used to quantitate pulmonary inflammation by tracking infiltrating PFC-loaded monocytes.[122] However, a practical concern/limitation relates to the application of fluorinated anesthesia gases in animal MRI experiments. Isoflurane ($CF_3CH_2ClOCHF_2$) potentially affects signal from PFC-labeled cells due to accumulation predominantly in subcutaneous fat regions and potentially from within the lungs after a period of gaseous anesthesia. However, to avoid possible false positive $^{19}$F signals from isoflurane, an option is to deliver injectable liquid anesthesia via mechanical pump and intraperitoneal catheter rather than inhaled anesthetics such as isoflurane.[179] Another option is the use of injectable anesthetics such as sodium pentobarbital, ketamine, xylazine, and thiopental in order to avoid the $^{19}$F signals due to isoflurane for preclinical cell tracking and $^{19}$F lung imaging.[70]

Hyperpolarized (HP) helium-3 ($^{3}$He) and xenon-129 ($^{129}$Xe) MRI of the lungs are a noninvasive imaging technique capable of measuring lung ventilation, gas exchange, and lung microstructure in both animals and humans.[180] HP gas MR also provides functional information about respiratory diseases, including chronic obstructive pulmonary disease, asthma, and cystic fibrosis.[181] Although $^{129}$Xe is cheaper than $^{3}$He, both $^{3}$He and $^{129}$Xe needs to prepare and process the gases. Thus, an attractive and economical alternative to HP gas MRI is functional MR imaging using inert fluorinated gases, such as sulfur hexafluoride ($SF_6$), hexafluoroethane ($C_2F_6$), and perfluoropropane (PFP) ($C_3F_8$), which are nontoxic and abundant.[182] Couch et al studied the feasibility of $^{19}$F 3D UTE for lung imaging of healthy volunteer with inert mixture of 79% PFP and 21% $O_2$.[183] Inert fluorinated gas MRI is a feasible pulmonary imaging technique with the potential of clinical transformation.

In $^{19}$F MR molecular imaging, nontargeted PFC agents have been designed for blood pool imaging and perfusion,[74,184] cellular labeling and tracking[7,185] cellular and tissue uptake imaging in inflammation, allograft rejection monitoring, among others.[59,186]

## Conclusion

Molecular imaging is a rapidly developing method that allows early tumor detection noninvasively and with high specificity. PFC NPs have been widely used in $^{19}$F MR molecular imaging because of their dense fluorine content and relatively bio-inert properties. In this article, we focused on the applications of $^{19}$F MRI in tumor molecular imaging. In addition to ligand-targeted imaging and tumor oxygenation quantification, PFC NPs have been explored for cell tracking, stimuli-responsive imaging and therapeutic drug delivery, as well as for the monitoring of therapy efficacy. We believe that $^{19}$F MRI will be widely used in research and clinical applications in the near future.

## Acknowledgments

This work was supported in part by the the National Natural Science Foundation of China (81627901, 81771903), Tou-Yan Innovation Team Program of Heilongjiang Province [2019-15], Natural Science Foundation of Heilongjiang Province, China (Grant No. JQ2020H002). China Scholarship Council (No. 201908230103), Heilongjiang Province Foundation for Returned Overseas Chinese Scholars (LC2016034), the Fourth Hospital of Harbin Medical University Fund for Distinguished Scholars (HYDSYJQ201601), and the Key Laboratory of Molecular Imaging Foundation (College of Heilongjiang Province).

## Disclosure

The authors report no conflicts of interest in this work.

## References

1. Bartusik D, Aebisher D. (19)F applications in drug development and imaging - a review. *Biomed Pharmacother*. 2014;68(6):813–817. doi:10.1016/j.biopha.2014.07.012

2. Longmaid HE, Adams DF, Neirinckx RD, et al. In vivo 19F NMR imaging of liver, tumor, and abscess in rats. Preliminary results. *Invest Radiol*. 1985;20(2):141–145. doi:10.1097/00004424-198503000-00009
3. Tirotta I, Dichiarante V, Pigliacelli C, et al. (19)F magnetic resonance imaging (MRI): from design of materials to clinical applications. *Chem Rev*. 2015;115(2):1106–1129. doi:10.1021/cr500286d
4. Krafft MP, Riess JG. Perfluorocarbons: life sciences and biomedical uses dedicated to the memory of Professor Guy Ourisson, a true RENAISSANCE man. *J Polym Sci A*. 2007;45(7):1185–1198. doi:10.1002/pola.21937
5. Krafft MP, Riess JG. Chemistry, physical chemistry, and uses of molecular fluorocarbon–hydrocarbon diblocks, triblocks, and related compounds–unique "apolar" components for self-assembled colloid and interface engineering. *Chem Rev*. 2009;109(5):1714–1792. doi:10.1021/cr800260k
6. Castro O, Nesbitt AE, Lyles D. Effect of a perfluorocarbon emulsion (Fluosol-DA) on reticuloendothelial system clearance function. *Am J Hematol*. 1984;16(1):15–21. doi:10.1002/ajh.2830160103
7. Janjic JM, Ahrens ET. Fluorine-containing nanoemulsions for MRI cell tracking. *Wiley Interdiscip Rev Nanomed Nanobiotechnol*. 2009;1(5):492–501. doi:10.1002/wnan.35
8. Spahn DR. Blood substitutes. Artificial oxygen carriers: perfluorocarbon emulsions. *Crit Care*. 1999;3(5):R93–97. doi:10.1186/cc364
9. Noveck RJ, Shannon EJ, Leese PT, et al. Randomized safety studies of intravenous perflubron emulsion. II. Effects on immune function in healthy volunteers. *Anesth Analg*. 2000;91(4):812–822. doi:10.1097/00000539-200010000-00009
10. Hu G, Lijowski M, Zhang H, et al. Imaging of Vx-2 rabbit tumors with alpha(nu)beta3-integrin-targeted 111In nanoparticles. *Int J Cancer*. 2007;120(9):1951–1957. doi:10.1002/ijc.22581
11. Riess JG. The design and development of improved fluorocarbon-based products for use in medicine and biology. *Artif Cells Blood Substit Immobil Biotechnol*. 1994;22(2):215–234. doi:10.3109/10731199409117416
12. Sadowski EA, Bennett LK, Chan MR, et al. Nephrogenic systemic fibrosis: risk factors and incidence estimation. *Radiology*. 2007;243(1):148–157. doi:10.1148/radiol.2431062144
13. Boyd AS, Zic JA, Abraham JL. Gadolinium deposition in nephrogenic fibrosing dermopathy. *J Am Acad Dermatol*. 2007;56(1):27–30. doi:10.1016/j.jaad.2006.10.048
14. Hu L, Chen J, Yang X, et al. Assessing intrarenal nonperfusion and vascular leakage in acute kidney injury with multinuclear (1) H/(19) F MRI and perfluorocarbon nanoparticles. *Magn Reson Med*. 2014;71(6):2186–2196. doi:10.1002/mrm.24851
15. Clark Jr LC, Gollan F. Survival of mammals breathing organic liquids equilibrated with oxygen at atmospheric pressure. *Science*. 1966;152(3730):1755–1756. doi:10.1126/science.152.3730.1755
16. Sloviter HA, Mukherji B. Prolonged retention in the circulation of emulsified lipid-coated perfluorochemicals. *Prog Clin Biol Res*. 1983;122:181–187.
17. Zuck TF, Riess JG, Biro GP. Current status of injectable oxygen carriers. *Crit Rev Clin Lab Sci*. 1994;31(4):295–324. doi:10.3109/10408369409084678
18. Hess JR. Alternative oxygen carriers. *Curr Opin Hematol*. 1996;3(6):492–497. doi:10.1097/00062752-199603060-00016
19. O'brien RN, Langlais AJ, Seufert WD. Diffusion coefficients of respiratory gases in a perfluorocarbon liquid. *Science*. 1982;217(4555):153–155. doi:10.1126/science.6806902
20. Zhang W, Ito Y, Berlin E, et al. Role of hypoxia during normal retinal vessel development and in experimental retinopathy of prematurity. *Invest Ophthalmol Vis Sci*. 2003;44(7):3119–3123. doi:10.1167/iovs.02-1122
21. Riess JG. Understanding the fundamentals of perfluorocarbons and perfluorocarbon emulsions relevant to in vivo oxygen delivery. *Artif Cells Blood Substit Immobil Biotechnol*. 2005;33(1):47–63. doi:10.1081/BIO-200046659
22. Yu JX, Kodibagkar VD, Cui W, et al. 19F: a versatile reporter for non-invasive physiology and pharmacology using magnetic resonance. *Curr Med Chem*. 2005;12(7):819–848.
23. Kodibagkar VD, Wang X, Mason RP. Physical principles of quantitative nuclear magnetic resonance oximetry. *Front Biosci*. 2008;13:1371–1384. doi:10.2741/2768
24. Laukemper-Ostendorf S, Scholz A, Burger K, et al. 19F-MRI of perflubron for measurement of oxygen partial pressure in porcine lungs during partial liquid ventilation. *Magn Reson Med*. 2002;47(1):82–89. doi:10.1002/mrm.10008
25. Chen J, Lanza GM, Wickline SA. Quantitative magnetic resonance fluorine imaging: today and tomorrow. *Wiley Interdiscip Rev Nanomed Nanobiotechnol*. 2010;2(4):431–440. doi:10.1002/wnan.87
26. Kaneda MM, Caruthers S, Lanza GM, et al. Perfluorocarbon nanoemulsions for quantitative molecular imaging and targeted therapeutics. *Ann Biomed Eng*. 2009;37(10):1922–1933. doi:10.1007/s10439-009-9643-z
27. Chen J, Pan H, Lanza GM, et al. Perfluorocarbon nanoparticles for physiological and molecular imaging and therapy. *Adv Chronic Kidney Dis*. 2013;20(6):466–478. doi:10.1053/j.ackd.2013.08.004
28. Schmieder AH, Caruthers SD, Keupp J, et al. Recent advances in (19) fluorine magnetic resonance imaging with perfluorocarbon emulsions. *Engineering (Beijing)*. 2015;1(4):475–489. doi:10.15302/J-ENG-2015103
29. Faas HM, Krupa JL, Taylor AJ, et al. Accelerated (19)F.MRI detection of matrix metalloproteinase-2/-9 through responsive deactivation of paramagnetic relaxation enhancement. *Contrast Media Mol Imaging*. 2019;2019:4826520. doi:10.1155/2019/4826520
30. Keupp J, Rahmer J, Grasslin I, et al. Simultaneous dual-nuclei imaging for motion corrected detection and quantification of 19F imaging agents. *Magn Reson Med*. 2011;66(4):1116–1122. doi:10.1002/mrm.22877
31. Otake Y, Soutome Y, Hirata K, et al. Double-tuned radiofrequency coil for (19)F and (1)H imaging. *Magn Reson Med Sci*. 2014;13(3):199–205. doi:10.2463/mrms.2013-0094
32. Villavalverde P, Rodriguez IR, Padro D, et al. A dual 1H/19F birdcage coil for small animals at 7 T MRI. *MRMPB*. 2019;32(1):79–87.
33. Constantinides C, Maguire M, Mcneill E, et al. Fast, quantitative, murine cardiac 19F MRI/MRS of PFCE-labeled progenitor stem cells and macrophages at 9.4T. *PLoS One*. 2018;13(1):e0190558. doi:10.1371/journal.pone.0190558
34. Hockett FD, Wallace KD, Schmieder AH, et al. Simultaneous dual frequency 1H and 19F open coil imaging of arthritic rabbit knee at 3T. *IEEE Trans Med Imaging*. 2011;30(1):22–27. doi:10.1109/TMI.2010.2056689
35. Ji Y, Waiczies H, Winter L, et al. Eight-channel transceiver RF coil array tailored for (1)H/(1)(9)F MR of the human knee and fluorinated drugs at 7.0 T. *NMR Biomed*. 2015;28(6):726–737. doi:10.1002/nbm.3300
36. Jacoby C, Temme S, Mayenfels F, et al. Probing different perfluorocarbons for in vivo inflammation imaging by 19F MRI: image reconstruction, biological half-lives and sensitivity. *NMR Biomed*. 2014;27(3):261–271. doi:10.1002/nbm.3059
37. Mastropietro A, De Bernardi E, Breschi GL, et al. Optimization of rapid acquisition with relaxation enhancement (RARE) pulse sequence parameters for 19F-MRI studies. *J Magn Reson Imaging*. 2014;40(1):162–170. doi:10.1002/jmri.24347
38. Kadayakkara DK, Damodaran K, Hitchens TK, et al. 19F spin–lattice relaxation of perfluoropolyethers: dependence on temperature and magnetic field strength (7.0–14.1 T). *J Magn Reson*. 2014;242:18–22. doi:10.1016/j.jmr.2014.01.014

39. Srinivas M, Cruz LJ, Bonetto F, et al. Customizable, multi-functional fluorocarbon nanoparticles for quantitative in vivo imaging using 19F MRI and optical imaging. *Biomaterials*. 2010;31(27):7070–7077. doi:10.1016/j.biomaterials.2010.05.069
40. Goette MJ, Keupp J, Rahmer J, et al. Balanced UTE-SSFP for 19F MR imaging of complex spectra. *Magn Reson Med*. 2015;74 (2):537–543. doi:10.1002/mrm.25437
41. Lamerichs R, Yildirim MJ, Nederveen A, et al. In vivo 3D 19 F fast spectroscopic imaging (F-uTSI) of angiogenesis on Vx-2 tumors in rabbits using targeted perfluorocarbon emulsions [M]. *Proc Int Soc Mag Reson Med*. 2017;18.
42. Van Heeswijk RB, Colotti R, Darcot E, et al. Chemical shift encoding (CSE) for sensitive fluorine-19 MRI of perfluorocarbons with complex spectra. *Magn Reson Med*. 2017;79(5):2724–2730.
43. Colotti R, Bastiaansen J, Wilson A, et al. Characterization of perfluorocarbon relaxation times and their influence on the optimization of fluorine-19 MRI at 3 tesla. *Magn Reson Med*. 2017;77 (6):2263–2271. doi:10.1002/mrm.26317
44. Peng Q, Yuan Y, Zhang H, et al. 19F CEST imaging probes for metal ion detection. *Org Biomol Chem*. 2017;15(30):6441–6446. doi:10.1039/C7OB01068K
45. Schoormans J, Calcagno C, Daal MRR, et al. An iterative sparse deconvolution method for simultaneous multicolor 19 F-MRI of multiple contrast agents. *Magn Reson Med*. 2020;83(1):228–239. doi:10.1002/mrm.27926
46. De Vries A, Moonen RPM, Yildirim M, et al. Relaxometric studies of gadolinium-functionalized perfluorocarbon nanoparticles for MR imaging. *Contrast Media Mol Imaging*. 2014;9(1):83–91. doi:10.1002/cmmi.1541
47. Flogel U, Ding Z, Hardung H, et al. In vivo monitoring of inflammation after cardiac and cerebral ischemia by fluorine magnetic resonance imaging. *Circulation*. 2008;118(2):140–148. doi:10.1161/CIRCULATIONAHA.107.737890
48. Guden-Silber T, Temme S, Jacoby C, et al. Biomedical (19)F MRI using perfluorocarbons. *Methods Mol Biol*. 2018;1718:235–257.
49. Makela AV, Gaudet JM, Foster PJ. Quantifying tumor associated macrophages in breast cancer: a comparison of iron and fluorine-based MRI cell tracking. *Sci Rep*. 2017;7:42109. doi:10.1038/srep42109
50. Zhou Z, Lu Z. Molecular imaging of the tumor microenvironment. *Adv Drug Deliv Rev*. 2017;113:24–48. doi:10.1016/j.addr.2016.07.012
51. Beik J, Jafariyan M, Montazerabadi A, et al. The benefits of folic acid-modified gold nanoparticles in CT-based molecular imaging: radiation dose reduction and image contrast enhancement. *Artif Cells Nanomed Biotechnol*. 2017;46(8):1993–2001.
52. Ta HT, Li Z, Hagemeyer CE, et al. Molecular imaging of activated platelets via antibody-targeted ultra-small iron oxide nanoparticles displaying unique dual MRI contrast. *Biomaterials*. 2017;134:31–42. doi:10.1016/j.biomaterials.2017.04.037
53. Wang K, Pan D, Schmieder AH, et al. Synergy between surface and core entrapped metals in a mixed manganese–gadolinium nanocolloid affords safer MR imaging of sparse biomarkers. *Nanomedicine*. 2015;11(3):601–609. doi:10.1016/j.nano.2014.12.009
54. Pham CTN, Mitchell LM, Huang J, et al. Variable antibody-dependent activation of complement by functionalized phospholipid nanoparticle surfaces. *J Biol Chem*. 2011;286 (1):123–130. doi:10.1074/jbc.M110.180760
55. Tennstaedt A, Mastropietro A, Nelles M, et al. In vivo fate imaging of intracerebral stem cell grafts in mouse brain. *PLoS One*. 2015;10 (12):e0144262. doi:10.1371/journal.pone.0144262
56. Himmelreich U, Weber R, Ramoscabrer P, et al. Improved stem cell MR detectability in animal models by modification of the inhalation gas. *Mol Imaging*. 2005;4(2):104–109. doi:10.1162/15353500200504196
57. Lanza GM, Wallace KD, Scott MJ, et al. A novel site-targeted ultrasonic contrast agent with broad biomedical application. *Circulation*. 1996;94(12):3334–3340. doi:10.1161/01.CIR.94.12.3334
58. Huynh E, Leung BY, Helfield BL, et al. In situ conversion of porphyrin microbubbles to nanoparticles for multimodality imaging. *Nat Nanotechnol*. 2015;10(4):325–332. doi:10.1038/nnano.2015.25
59. Hitchens TK, Ye Q, Eytan DF, et al. 19F MRI detection of acute allograft rejection with in vivo perfluorocarbon labeling of immune cells. *Magn Reson Med*. 2011;65(4):1144–1153. doi:10.1002/mrm.22702
60. Srinivas M, Turner MS, Janjic JM, et al. In vivo cytometry of antigen-specific t cells using 19F MRI. *Magn Reson Med*. 2009;62(3):747–753. doi:10.1002/mrm.22063
61. Zhou H-F, Yan H, Senpan A, et al. Suppression of inflammation in a mouse model of rheumatoid arthritis using targeted lipase-labile fumagillin prodrug nanoparticles. *Biomaterials*. 2012;33 (33):8632–8640. doi:10.1016/j.biomaterials.2012.08.005
62. Caruthers SD, Cyrus T, Winter PM, et al. Anti-angiogenic perfluorocarbon nanoparticles for diagnosis and treatment of atherosclerosis. *Wiley Interdiscip Rev Nanomed Nanobiotechnol*. 2009;1(3):311–323. doi:10.1002/wnan.9
63. Lanza GM, Winter PM, Caruthers SD, et al. Theragnostics for tumor and plaque angiogenesis with perfluorocarbon nanoemulsions. *Angiogenesis*. 2010;13(2):189–202. doi:10.1007/s10456-010-9166-0
64. Pan D, Caruthers SD, Chen J, et al. Nanomedicine strategies for molecular targets with MRI and optical imaging. *Future Med Chem*. 2010;2(3):471–490. doi:10.4155/fmc.10.5
65. Lanza GM, Lorenz CH, Fischer SE, et al. Enhanced detection of thrombi with a novel fibrin-targeted magnetic resonance imaging agent. *Acad Radiol*. 1998;5(Suppl 1):SS173–174. doi:10.1016/S1076-6332(98)80097-4
66. Lanza GM, Trousil RL, Wallace KD, et al. In vitro characterization of a novel, tissue-targeted ultrasonic contrast system with acoustic microscopy. *J Acoust Soc Am*. 1998;104(6):3665–3672. doi:10.1121/1.423948
67. Lanza GM, Winter PM, Caruthers SD, et al. Magnetic resonance molecular imaging with nanoparticles. *J Nucl Cardiol*. 2004;11 (6):733–743. doi:10.1016/j.nuclcard.2004.09.002
68. Lanza GM, Yu X, Winter PM, et al. Targeted antiproliferative drug delivery to vascular smooth muscle cells with a magnetic resonance imaging nanoparticle contrast agent: implications for rational therapy of restenosis. *Circulation*. 2002;106(22):2842–2847. doi:10.1161/01.CIR.0000044020.27990.32
69. Ruiz-Cabello J, Barnett BP, Bottomley PA, et al. Fluorine (19F) MRS and MRI in biomedicine. *NMR Biomed*. 2011;24(2):114–129. doi:10.1002/nbm.1570
70. Ahrens ET, Zhong J. In vivo MRI cell tracking using perfluorocarbon probes and fluorine-19 detection. *NMR Biomed*. 2013;26 (7):860–871. doi:10.1002/nbm.2948
71. Du W, Xu Z, NyströM AM, et al. 19F- and fluorescently labeled micelles as nanoscopic assemblies for chemotherapeutic delivery. *Bioconjug Chem*. 2008;19(12):2492–2498. doi:10.1021/bc800396h
72. Langereis S, Keupp J, Van Velthoven JL, et al. A temperature-sensitive liposomal 1H CEST and 19F contrast agent for MR image-guided drug delivery. *J Am Chem Soc*. 2009;131 (4):1380–1381. doi:10.1021/ja8087532
73. Partlow KC, Lanza GM, Wickline SA. Exploiting lipid raft transport with membrane targeted nanoparticles: a strategy for cytosolic drug delivery. *Biomaterials*. 2008;29(23):3367–3375. doi:10.1016/j.biomaterials.2008.04.030
74. Morawski AM, Winter PM, Crowder KC, et al. Targeted nanoparticles for quantitative imaging of sparse molecular epitopes with MRI. *Magn Reson Med*. 2004;51(3):480–486. doi:10.1002/mrm.20010

75. Flacke S, Fischer S, Scott MJ, et al. Novel MRI contrast agent for molecular imaging of fibrin: implications for detecting vulnerable plaques. *Circulation*. 2001;104(11):1280–1285. doi:10.1161/hc3601.094303
76. Winter PM, Caruthers SD, Kassner A, et al. Molecular imaging of angiogenesis in nascent Vx-2 rabbit tumors using a novel alpha(nu) beta3-targeted nanoparticle and 1.5 tesla magnetic resonance imaging. *Cancer Res*. 2003;63(18):5838–5843.
77. Diou O, Fattal E, Delplace V, et al. RGD decoration of PEGylated polyester nanocapsules of perfluorooctyl bromide for tumor imaging: influence of pre or post-functionalization on capsule morphology. *Eur J Pharm Biopharm*. 2014;87(1):170–177. doi:10.1016/j.ejpb.2013.12.003
78. Schmieder AH, Winter PM, Williams TA, et al. Molecular MR imaging of neovascular progression in the Vx2 tumor with alphavbeta3-targeted paramagnetic nanoparticles. *Radiology*. 2013;268(2):470–480. doi:10.1148/radiol.13120789
79. Giraudeau C, Geffroy F, Meriaux S, et al. 19F molecular MR imaging for detection of brain tumor angiogenesis: in vivo validation using targeted PFOB nanoparticles. *Angiogenesis*. 2013;16(1):171–179. doi:10.1007/s10456-012-9310-0
80. Xuan J, Chen Y, Zhu L, et al. Ultrasound molecular imaging with cRGD-PLGA-PFOB nanoparticles for liver fibrosis staging in a rat model. *Oncotarget*. 2017;8(65):108676–108691. doi:10.18632/oncotarget.21358
81. Vu-Quang H, Vinding MS, Nielsen T, et al. Theranostic tumor targeted nanoparticles combining drug delivery with dual near infrared and (19)F magnetic resonance imaging modalities. *Nanomedicine*. 2016;12(7):1873–1884. doi:10.1016/j.nano.2016.04.010
82. Li K, Liu Y, Zhang S, et al. Folate receptor-targeted ultrasonic PFOB nanoparticles: synthesis, characterization and application in tumor-targeted imaging. *Int J Mol Med*. 2017;39(6):1505–1515. doi:10.3892/ijmm.2017.2975
83. Hu Y, Wang Y, Jiang J, et al. Preparation and characterization of novel perfluorooctyl bromide nanoparticle as ultrasound contrast agent via layer-by-layer self-assembly for folate-receptor-mediated tumor imaging. *Biomed Res Int*. 2016;2016:6381464. doi:10.1155/2016/6381464
84. Liu X, Zhao J, Guo D, et al. Synthesis and evaluation of perfluorooctylbromide nanoparticles modified with a folate receptor for targeting ovarian cancer: in vitro and in vivo experiments. *Int J Clin Exp Med*. 2015;8(6):10122–10131.
85. Chen WT, Kang ST, Lin JL, et al. Targeted tumor theranostics using folate-conjugated and camptothecin-loaded acoustic nanodroplets in a mouse xenograft model. *Biomaterials*. 2015;53:699–708. doi:10.1016/j.biomaterials.2015.02.122
86. Chen H, Chen L, Liang R, et al. Ultrasound and magnetic resonance molecular imaging of atherosclerotic neovasculature with perfluorocarbon magnetic nanocapsules targeted against vascular endothelial growth factor receptor 2 in rats. *Mol Med Rep*. 2017;16(5):5986–5996. doi:10.3892/mmr.2017.7314
87. Lother A, Deng L, Huck M, et al. Endothelial cell mineralocorticoid receptors oppose VEGF-induced gene expression and angiogenesis. *J Endocrinol*. 2019;240(1):15–26. doi:10.1530/JOE-18-0494
88. Waters EA, Chen J, Yang X, et al. Detection of targeted perfluorocarbon nanoparticle binding using 19F diffusion weighted MR spectroscopy. *Magn Reson Med*. 2008;60(5):1232–1236. doi:10.1002/mrm.21794
89. Xu X, Zhang R, Liu F, et al. 19F MRI in orthotopic cancer model via intratracheal administration of αvβ3-targeted perfluorocarbon nanoparticles. *Nanomedicine*. 2018;13(20):2551–2562. doi:10.2217/nnm-2018-0051
90. Bae PK, Jung J, Lim SJ, et al. Bimodal perfluorocarbon nanoemulsions for nasopharyngeal carcinoma targeting. *Mol Imaging Biol*. 2013;15(4):401–410. doi:10.1007/s11307-013-0622-2
91. Patel J, Amrutiya J, Bhatt P, et al. Targeted delivery of monoclonal antibody conjugated docetaxel loaded PLGA nanoparticles into EGFR overexpressed lung tumour cells. *J Microencapsul*. 2018;35(2):204–217. doi:10.1080/02652048.2018.1453560
92. Sok JC, Coppelli FM, Thomas SM, et al. Mutant epidermal growth factor receptor (EGFRvIII) contributes to head and neck cancer growth and resistance to EGFR targeting. *Clin Cancer Res*. 2006;12(17):5064–5073. doi:10.1158/1078-0432.CCR-06-0913
93. Wang Y, Zhou J, Qiu L, et al. Cisplatin-alginate conjugate liposomes for targeted delivery to EGFR-positive ovarian cancer cells. *Biomaterials*. 2014;35(14):4297–4309.
94. Li F, Mei H, Gao Y, et al. Co-delivery of oxygen and erlotinib by aptamer-modified liposomal complexes to reverse hypoxia-induced drug resistance in lung cancer. *Biomaterials*. 2017;145:56–71. doi:10.1016/j.biomaterials.2017.08.030
95. Tatum JL, Kelloff GJ, Gillies RJ, et al. Hypoxia: importance in tumor biology, noninvasive measurement by imaging, and value of its measurement in the management of cancer therapy. *Int J Radiat Biol*. 2006;82(10):699–757. doi:10.1080/09553000601002324
96. Zhao D, Jiang L, Mason RP. Measuring changes in tumor oxygenation. *Methods Enzymol*. 2004;386:378–418.
97. Spiess BD. Perfluorocarbon emulsions as a promising technology: a review of tissue and vascular gas dynamics. *J Appl Physiol (1985)*. 2009;106(4):1444–1452. doi:10.1152/japplphysiol.90995.2008
98. Yu JX, Kodibagkar VD, Cui W, et al. 19F: a versatile reporter for non-invasive physiology and pharmacology using magnetic resonance. *Curr Med Chem*. 2005;12(7):819–848. doi:10.2174/0929867053507342
99. Sloviter HA, Kamimoto T. Erythrocyte substitute for perfusion of brain. *Nature*. 1967;216(5114):458–460. doi:10.1038/216458a0
100. Faithfull NS, King CE, Cain SM. Peripheral vascular responses to fluorocarbon administration. *Microvasc Res*. 1987;33(2):183–193. doi:10.1016/0026-2862(87)90016-1
101. Christensen CW, Reeves WC, Lassar TA, et al. Inadequate subendocardial oxygen delivery during perfluorocarbon perfusion in a canine model of ischemia. *Am Heart J*. 1988;115(1 Pt 1):30–37. doi:10.1016/0002-8703(88)90514-5
102. Brown JM, Wilson WR. Exploiting tumour hypoxia in cancer treatment. *Nat Rev Cancer*. 2004;4(6):437–447. doi:10.1038/nrc1367
103. Vaupel P, Thews O, Hoeckel M. Treatment resistance of solid tumors: role of hypoxia and anemia. *Med Oncol*. 2001;18(4):243–259. doi:10.1385/MO:18:4:243
104. Xie D, Kim S, Kohli V, et al. Hypoxia-responsive 19F MRI probes with improved redox properties and biocompatibility. *Inorg Chem*. 2017;56(11):6429–6437. doi:10.1021/acs.inorgchem.7b00500
105. Parhami P, Fung B. Fluorine-19 relaxation study of perfluoro chemicals as oxygen carriers. *J Phys Chem*. 1983;87(11):1928–1931.
106. Zhao D, Constantinescu A, Hahn EW, et al. Tumor oxygen dynamics with respect to growth and respiratory challenge: investigation of the dunning prostate R3327-HI tumor 1. *Radiat Res*. 2001;156(5):510–520. doi:10.1667/0033-7587(2001)156[0510:TODWRT]2.0.CO;2
107. Song Y, Constantinescu A, Mason RP. Dynamic breast tumor oximetry: the development of prognostic radiology. *Technol Cancer Res Treat*. 2002;1(6):471–478. doi:10.1177/153303460200100607
108. Zhao D, Constantinescu A, Chang CH, et al. Correlation of tumor oxygen dynamics with radiation response of the dunning prostate R3327-HI tumor 1. *Radiat Res*. 2003;159(5):621–631. doi:10.1667/0033-7587(2003)159[0621:COTODW]2.0.CO;2
109. Sc BPJVDSM, Heerschap A, Simonetti AW, et al. Characterization and validation of noninvasive oxygen tension measurements in human glioma xenografts by 19F-MR relaxometry. *Int J Radiat Oncol Biol Phys*. 1999;44(3):649–658. doi:10.1016/S0360-3016(98)00555-0

110. Liu S, Shah S, Wilmes LJ, et al. Quantitative tissue oxygen measurement in multiple organs using 19F MRI in a rat model. *Magn Reson Med*. 2011;66(6):1722–1730. doi:10.1002/mrm.22968
111. Shi Y, Oeh J, Easthamanderson J, et al. Mapping in vivo tumor oxygenation within viable tumor by 19F-MRI and multispectral analysis. *Neoplasia*. 2013;15(11):1241–1250. doi:10.1593/neo.131468
112. Hunjan S, Zhao D, Constantinescu A, et al. Tumor oximetry: demonstration of an enhanced dynamic mapping procedure using fluorine-19 echo planar magnetic resonance imaging in the Dunning prostate R3327-AT1 rat tumor. *Int J Radiat Oncol Biol Phys*. 2001;49(4):1097–1108. doi:10.1016/S0360-3016(00)01460-7
113. Magat J, Jordan BF, Cron GO, et al. Noninvasive mapping of spontaneous fluctuations in tumor oxygenation using 19F MRI. *Med Phys*. 2010;37(10):5434–5441. doi:10.1118/1.3484056
114. Jordan BF, Cron GO, Gallez B. Rapid monitoring of oxygenation by 19F magnetic resonance imaging: simultaneous comparison with fluorescence quenching. *Magn Reson Med*. 2009;61(3):634–638. doi:10.1002/mrm.21594
115. Kadayakkara DK, Janjic JM, Pusateri LK, et al. In vivo observation of intracellular oximetry in perfluorocarbon-labeled glioma cells and chemotherapeutic response in the CNS using fluorine-19 MRI. *Magn Reson Med*. 2010;64(5):1252–1259. doi:10.1002/mrm.22506
116. Ahrens ET, Bulte JW. Tracking immune cells in vivo using magnetic resonance imaging. *Nat Rev Immunol*. 2013;13(10):755–763. doi:10.1038/nri3531
117. Ahrens ET, Helfer BM, O'hanlon CF, et al. Clinical cell therapy imaging using a perfluorocarbon tracer and fluorine-19 MRI. *Magn Reson Med*. 2014;72(6):1696–1701. doi:10.1002/mrm.25454
118. Boehm-Sturm P, Mengler L, Wecker S, et al. In vivo tracking of human neural stem cells with 19F magnetic resonance imaging. *PLoS One*. 2011;6(12):e29040. doi:10.1371/journal.pone.0029040
119. Bulte JW. Hot spot MRI emerges from the background. *Nat Biotechnol*. 2005;23(8):945–946.
120. Ye YX, Basse-Lusebrink TC, Arias-Loza PA, et al. Monitoring of monocyte recruitment in reperfused myocardial infarction with intramyocardial hemorrhage and microvascular obstruction by combined fluorine 19 and proton cardiac magnetic resonance imaging. *Circulation*. 2013;128(17):1878–1888. doi:10.1161/CIRCULATIONAHA.113.000731
121. Van Heeswijk RB, De Blois J, Kania G, et al. Selective in vivo visualization of immune-cell infiltration in a mouse model of autoimmune myocarditis by fluorine-19 cardiac magnetic resonance. *Circ Cardiovasc Imaging*. 2013;6(2):277–284. doi:10.1161/CIRCIMAGING.112.000125
122. Ebner B, Behm P, Jacoby C, et al. Early assessment of pulmonary inflammation by 19F MRI in vivo. *Circ Cardiovasc Imaging*. 2010;3(2):202–210. doi:10.1161/CIRCIMAGING.109.902312
123. Van Heeswijk RB, Pellegrin M, Flogel U, et al. Fluorine MR imaging of inflammation in atherosclerotic plaque in vivo. *Radiology*. 2015;275(2):421–429. doi:10.1148/radiol.14141371
124. Flogel U, Burghoff S, Van Lent PL, et al. Selective activation of adenosine A2A receptors on immune cells by a CD73-dependent prodrug suppresses joint inflammation in experimental rheumatoid arthritis. *Sci Transl Med*. 2012;4(146):146ra108. doi:10.1126/scitranslmed.3003717
125. Balducci A, Wen Y, Zhang Y, et al. A novel probe for the non-invasive detection of tumor-associated inflammation. *Oncoimmunology*. 2013;2(2):e23034. doi:10.4161/onci.23034
126. Constantinides C, Basnett P, Lukasiewicz B, et al. In vivo tracking and (1)H/(19)F magnetic resonance imaging of biodegradable polyhydroxyalkanoate/polycaprolactone blend scaffolds seeded with labeled cardiac stem cells. *ACS Appl Mater Interfaces*. 2018;10(30):25056–25068. doi:10.1021/acsami.8b06096
127. Fink C, Gaudet JM, Fox MS, et al. 19F-perfluorocarbon-labeled human peripheral blood mononuclear cells can be detected in vivo using clinical MRI parameters in a therapeutic cell setting. *Sci Rep*. 2018;8(1):590. doi:10.1038/s41598-017-19031-0
128. Constantinides C, Mcneill E, Carnicer R, et al. Improved cellular uptake of perfluorocarbon nanoparticles for in vivo murine cardiac (19)F MRS/MRI and temporal tracking of progenitor cells. *Nanomedicine*. 2019;18:391–401. doi:10.1016/j.nano.2018.10.014
129. Ramos IT, Henningsson M, Nezafat M, et al. Simultaneous assessment of cardiac inflammation and extracellular matrix remodeling after myocardial infarction. *Circ Cardiovasc Imaging*. 2018;11(11). doi:10.1161/CIRCIMAGING.117.007453.
130. Gaudet JM, Ribot EJ, Chen Y, et al. Tracking the fate of stem cell implants with fluorine-19 MRI. *PLoS One*. 2015;10(3):0118544. doi:10.1371/journal.pone.0118544
131. Manzo T, Heslop HE, Rooney CM. Antigen-specific T cell therapies for cancer. *Hum Mol Genet*. 2015;24(R1):R67–73. doi:10.1093/hmg/ddv270
132. Gonzales C, Yoshihara HA, Dilek N, et al. In-vivo detection and tracking of T cells in various organs in a melanoma tumor model by 19F-fluorine MRS/MRI. *PLoS One*. 2016;11(10):e0164557. doi:10.1371/journal.pone.0164557
133. Gaudet JM, Hamilton AM, Chen Y, et al. Application of dual 19F and iron cellular MRI agents to track the infiltration of immune cells to the site of a rejected stem cell transplant. *Magn Reson Med*. 2017;78(2):713–720. doi:10.1002/mrm.26400
134. Makela AV, Foster PJ. Imaging macrophage distribution and density in mammary tumors and lung metastases using fluorine-19 MRI cell tracking. *Magn Reson Med*. 2018;80(3):1138–1147. doi:10.1002/mrm.27081
135. Ribot EJ, Gaudet JM, Chen Y, et al. In vivo MR detection of fluorine-labeled human MSC using the bSSFP sequence. *Int J Nanomedicine*. 2014;9(1):1731–1739. doi:10.2147/IJN.S59127
136. Boehmsturm P, Aswendt M, Minassian A, et al. A multi-modality platform to image stem cell graft survival in the naïve and stroke-damaged mouse brain. *Biomaterials*. 2014;35(7):2218–2226. doi:10.1016/j.biomaterials.2013.11.085
137. Fink C, Smith M, Gaudet JM, et al. Fluorine-19 cellular MRI detection of in vivo dendritic cell migration and subsequent induction of tumor antigen-specific immunotherapeutic response. *Mol Imaging Biol*. 2019;1–13.
138. Partlow KC, Chen J, Brant JA, et al. 19F magnetic resonance imaging for stem/progenitor cell tracking with multiple unique perfluorocarbon nanobeacons. *FASEB J*. 2007;21(8):1647–1654. doi:10.1096/fj.06-6505com
139. Constantinides C, Mean R, Janssen BJ. Effects of isoflurane anesthesia on the cardiovascular function of the C57BL/6 mouse. *ILAR J*. 2011;52(3):e21.
140. Constantinides C, Maguire ML, Stork L, et al. Temporal accumulation and localization of isoflurane in the C57BL/6 mouse and assessment of its potential contamination in (19) F MRI with perfluoro-crown-ether-labeled cardiac progenitor cells at 9.4 Tesla. *J Magn Reson Imaging*. 2017;45(6):1659–1667. doi:10.1002/jmri.25564
141. Van Heeswijk RB, Pilloud Y, Flogel U, et al. Fluorine-19 magnetic resonance angiography of the mouse. *PLoS One*. 2012;7(7):42236. doi:10.1371/journal.pone.0042236
142. Rapoport N, Gao Z, Kennedy A. Multifunctional nanoparticles for combining ultrasonic tumor imaging and targeted chemotherapy. *J Natl Cancer Inst*. 2007;99(14):1095–1106. doi:10.1093/jnci/djm043
143. Rapoport N, Christensen DA, Kennedy AM, et al. Cavitation properties of block copolymer stabilized phase-shift nanoemulsions used as drug carriers. *Ultrasound Med Biol*. 2010;36(3):419–429. doi:10.1016/j.ultrasmedbio.2009.11.009

144. Rapoport N, Pitt WG, Sun H, et al. Drug delivery in polymeric micelles: from in vitro to in vivo. *J Control Release*. 2003;91(1–2):85–95. doi:10.1016/S0168-3659(03)00218-9
145. Rapoport N, Gupta R, Kim YS, et al. Polymeric micelles and nanoemulsions as tumor-targeted drug carriers: insight through intravital imaging. *J Control Release*. 2015;206:153–160. doi:10.1016/j.jconrel.2015.03.010
146. Ferrara N, Hillan KJ, Gerber HP, et al. Discovery and development of bevacizumab, an anti-VEGF antibody for treating cancer. *Nat Rev Drug Discov*. 2004;3(5):391–400. doi:10.1038/nrd1381
147. Folkman J. Angiogenesis and apoptosis. *Semin Cancer Biol*. 2003;13(2):159–167. doi:10.1016/S1044-579X(02)00133-5
148. Winter PM, Schmieder AH, Caruthers SD, et al. Minute dosages of alpha(nu)beta3-targeted fumagillin nanoparticles impair Vx-2 tumor angiogenesis and development in rabbits. *FASEB J*. 2008;22(8):2758–2767. doi:10.1096/fj.07-103929
149. Shin SH, Park EJ, Min C, et al. Tracking perfluorocarbon nanoemulsion delivery by 19F MRI for precise high intensity focused ultrasound tumor ablation. *Theranostics*. 2017;7(3):562–572. doi:10.7150/thno.16895
150. Niu D, Wang X, Li Y, et al. Facile synthesis of magnetite/perfluorocarbon co-loaded organic/inorganic hybrid vesicles for dual-modality ultrasound/magnetic resonance imaging and imaging-guided high-intensity focused ultrasound ablation. *Adv Mater*. 2013;25(19):2686–2692. doi:10.1002/adma.201204316
151. Gupta R, Cvetkovic D, Ma CM, et al. Targeted approach for prostate cancer treatment: synthesis and characterization of docetaxel-loaded perfluorocarbon nanodroplets. *J Cancer Sci Clin Oncol*. 2014;1(1).
152. Waldhauer I, Steinle A. NK cells and cancer immunosurveillance. *Oncogene*. 2008;27(45):5932–5943. doi:10.1038/onc.2008.267
153. Bouchlaka MN, Ludwig KD, Gordon JW, et al. (19)F-MRI for monitoring human NK cells in vivo. *Oncoimmunology*. 2016;5(5):e1143996. doi:10.1080/2162402X.2016.1143996
154. Neuschmelting V, Lockau H, Ntziachristos V, et al. Lymph node micrometastases and in-transit metastases from melanoma: in vivo detection with multispectral optoacoustic imaging in a mouse model. *Radiology*. 2016;280(1):137–150. doi:10.1148/radiol.2016160191
155. Swider E, Daoudi K, Staal AHJ, et al. Clinically-applicable perfluorocarbon-loaded nanoparticles for in vivo photoacoustic, (19) F magnetic resonance and fluorescent imaging. *Nanotheranostics*. 2018;2(3):258–268. doi:10.7150/ntno.26208
156. Ding Z, Sun H, Ge S, et al. Furin-controlled Fe3O4 nanoparticle aggregation and 19F signal "Turn-On" for precise MR imaging of tumors. *Adv Funct Mater*. 2019;29(43):1903860. doi:10.1002/adfm.201903860
157. Huang P, Guo W, Yang G, et al. Fluorine meets amine: reducing microenvironment-induced amino-activatable nanoprobes for (19) F-magnetic resonance imaging of biothiols. *ACS Appl Mater Interfaces*. 2018;10(22):18532–18542. doi:10.1021/acsami.8b03764
158. Akazawa K, Sugihara F, Nakamura T, et al. Highly sensitive detection of caspase-3/7 activity in living mice using enzyme-responsive 19F MRI nanoprobes. *Bioconjug Chem*. 2018;29(5):1720–1728. doi:10.1021/acs.bioconjchem.8b00167
159. Yuan Y, Ge S, Sun H, et al. Intracellular self-assembly and disassembly of 19F nanoparticles confer respective "off" and "on" 19F NMR/MRI signals for legumain activity detection in zebrafish. *ACS Nano*. 2015;9(5):5117–5124. doi:10.1021/acsnano.5b00287
160. Guo C, Zhang Y, Li Y, et al. 19F MRI nanoprobes for the turn-on detection of phospholipase A2 with a low background. *Anal Chem*. 2019;91(13):8147–8153. doi:10.1021/acs.analchem.9b00435
161. Yuan Y, Sun H, Ge S, et al. Controlled intracellular self-assembly and disassembly of 19F nanoparticles for MR imaging of caspase 3/7 in zebrafish. *ACS Nano*. 2015;9(1):761–768. doi:10.1021/nn5062657
162. Merkwitz C, Blaschuk O, Winkler J, et al. Advantages and limitations of salmon-gal/tetrazolium salt histochemistry for the detection of LacZ reporter gene activity in murine epithelial tissue. *J Histochem Cytochem*. 2017;65(4):197–206. doi:10.1369/0022155417690336
163. Nakamura T, Matsushita H, Sugihara F, et al. Activatable 19F MRI nanoparticle probes for the detection of reducing environments. *Angew Chem Int Ed Engl*. 2015;54(3):1007–1010. doi:10.1002/anie.201409365
164. Kadakia RT, Xie D, Martinez D, et al. A dual-responsive probe for detecting cellular hypoxia using 19F magnetic resonance and fluorescence. *Chem Commun (Camb)*. 2019;55(60):8860–8863. doi:10.1039/C9CC00375D
165. Fu C, Tang J, Pye A, et al. Fluorinated glycopolymers as reduction-responsive (19)F MRI agents for targeted imaging of cancer. *Biomacromolecules*. 2019;20(5):2043–2050. doi:10.1021/acs.biomac.9b00241
166. Akazawa K, Sugihara ;F, Minoshima M, et al.Sensing caspase-1 activity using activatable 19F MRI nanoprobes with improved turn-on kinetics. *Chem Commun (Camb)*. 2018;54(83):11785–11788. doi:10.1039/C8CC05381B
167. Stubbs M, Mcsheehy PM, Griffiths JR, et al. Causes and consequences of tumour acidity and implications for treatment. *Mol Med Today*. 2000;6(1):15–19. doi:10.1016/S1357-4310(99)01615-9
168. Neri D, Supuran CT. Interfering with pH regulation in tumours as a therapeutic strategy. *Nat Rev Drug Discov*. 2011;10(10):767–777. doi:10.1038/nrd3554
169. Huang X, Huang G, Zhang S, et al. Multi-chromatic pH-activatable 19F-MRI nanoprobes with binary ON/OFF pH transitions and chemical-shift barcodes. *Angew Chem Int Ed Engl*. 2013;52(31):8074–8078. doi:10.1002/anie.201301135
170. Guo C, Xu S, Arshad A, et al. A pH-responsive nanoprobe for turn-on 19 F-magnetic resonance imaging. *Chem Commun (Camb)*. 2018;54(70):9853–9856. doi:10.1039/C8CC06129G
171. Zhang C, Li L, Han FY, et al. Integrating fluorinated polymer and manganese-layered double hydroxide nanoparticles as pH-activated (19) F MRI agents for specific and sensitive detection of breast cancer. *Small*. 2019;15(36):e1902309. doi:10.1002/smll.201902309
172. Wang K, Peng H, Thurecht KJ, et al. pH-responsive star polymer nanoparticles: potential 19F MRI contrast agents for tumour-selective imaging. *Polym Chem*. 2013;4(16):4480. doi:10.1039/c3py00654a
173. Chen S, Yang Y, Li H, et al. pH-Triggered Au-fluorescent mesoporous silica nanoparticles for 19 F MR/fluorescent multimodal cancer cellular imaging. *Chem Commun (Camb)*. 2014;50(3):283–285. doi:10.1039/C3CC47324D
174. Temme S, Grapentin C, Quast C, et al. Noninvasive imaging of early venous thrombosis by 19F magnetic resonance imaging with targeted perfluorocarbon nanoemulsions. *Circulation*. 2015;131(16):1405–1414. doi:10.1161/CIRCULATIONAHA.114.010962
175. Waters EA, Chen J, Allen JS, et al. Detection and quantification of angiogenesis in experimental valve disease with integrin-targeted nanoparticles and 19-fluorine MRI/MRS. *J Cardiovasc Magn Reson*. 2008;10:43. doi:10.1186/1532-429X-10-43
176. Kuethe DO, Caprihan A, Fukushima E, et al. Imaging lungs using inert fluorinated gases. *Magn Reson Med*. 1998;39(1):85–88. doi:10.1002/mrm.1910390114
177. Schreiber WG, Eberle B, Laukemper-Ostendorf S, et al. Dynamic (19)F-MRI of pulmonary ventilation using sulfur hexafluoride (SF(6)) gas. *Magn Reson Med*. 2001;45(4):605–613. doi:10.1002/mrm.1082
178. Schmieder AH, Wang K, Zhang H, et al. Characterization of early neovascular response to acute lung ischemia using simultaneous (19)F/(1)H MR molecular imaging. *Angiogenesis*. 2014;17(1):51–60. doi:10.1007/s10456-013-9377-2

179. Srinivas M, Morel PA, Ernst LA, et al. Fluorine-19 MRI for visualization and quantification of cell migration in a diabetes model. *Magn Reson Med*. 2007;58(4):725–734. doi:10.1002/mrm.21352
180. Altes TA, Salerno M. Hyperpolarized gas MR imaging of the lung. *J Thorac Imaging*. 2004;19(4):250–258. doi:10.1097/01.rti.0000142837.52729.38
181. Couch MJ, Blasiak B, Tomanek B, et al. Hyperpolarized and inert gas MRI: the future. *Mol Imaging Biol*. 2015;17(2):149–162. doi:10.1007/s11307-014-0788-2
182. Halaweish AF, Moon RE, Foster WM, et al. Perfluoropropane gas as a magnetic resonance lung imaging contrast agent in humans. *Chest*. 2013;144(4):1300–1310. doi:10.1378/chest.12-2597
183. Couch MJ, Ball IK, Li T, et al. Pulmonary ultrashort echo time 19F MR imaging with inhaled fluorinated gas mixtures in healthy volunteers: feasibility. *Radiology*. 2013;269(3):903–909. doi:10.1148/radiol.13130609
184. Neubauer AM, Caruthers SD, Hockett FD, et al. Fluorine cardiovascular magnetic resonance angiography in vivo at 1.5 T with perfluorocarbon nanoparticle contrast agents. *J Cardiovasc Magn Reson*. 2007;9(3):565–573. doi:10.1080/10976640600945481
185. Ahrens ET, Flores R, Xu H, et al. In vivo imaging platform for tracking immunotherapeutic cells. *Nat Biotechnol*. 2005;23(8):983–987. doi:10.1038/nbt1121
186. Zhang H, Zhang L, Myerson J, et al. Quantifying the evolution of vascular barrier disruption in advanced atherosclerosis with semi-permanent nanoparticle contrast agents. *PLoS One*. 2011;6(10):e26385. doi:10.1371/journal.pone.0026385
187. Ruiz-Cabello J, Walczak P, Kedziorek DA, et al. In vivo "hot spot" MR imaging of neural stem cells using fluorinated nanoparticles. *Magn Reson Med*. 2008;60(6):1506–1511. doi:10.1002/mrm.21783
188. Kislukhin AA, Xu H, Adams SR, et al. Paramagnetic fluorinated nanoemulsions for sensitive cellular fluorine-19 magnetic resonance imaging. *Nat Mater*. 2016;15(6):662–668. doi:10.1038/nmat4585
189. Koshkina O, Lajoinie G, Baldelli F, et al. Multicore liquid perfluorocarbon-loaded multimodal nanoparticles for stable ultrasound and ~(19)F MRI applied to in vivo cell tracking. *Adv Funct Mater*. 2019;29(19):1806485.1806481–1806485.1806414.
190. Mason RP, Antich PP, Babcock EE, et al. Perfluorocarbon imaging in vivo: a 19F MRI study in tumor-bearing mice. *Magn Reson Imaging*. 1989;7(5):475–485. doi:10.1016/0730-725X(89)90402-5
191. Meyer KL, Carvlin MJ, Mukherji B, et al. Fluorinated blood substitute retention in the rat measured by fluorine-19 magnetic resonance imaging. *Invest Radiol*. 1992;27(8):620–627. doi:10.1097/00004424-199208000-00012
192. Morawski AM, Winter PM, Yu X, et al. Quantitative "magnetic resonance immunohistochemistry" with ligand-targeted (19)F nanoparticles. *Magn Reson Med*. 2004;52(6):1255–1262. doi:10.1002/mrm.20287
193. Zhou ZX, Zhang BG, Zhang H, et al. Drug packaging and delivery using perfluorocarbon nanoparticles for targeted inhibition of vascular smooth muscle cells. *Acta Pharmacol Sin*. 2009;30(11):1577–1584. doi:10.1038/aps.2009.146
194. Ahrens ET, Young WB, Xu H, et al. Rapid quantification of inflammation in tissue samples using perfluorocarbon emulsion and fluorine-19 nuclear magnetic resonance. *Biotechniques*. 2011;50(4):229–234. doi:10.2144/000113652
195. Goette MJ, Schmieder AH, Williams TA, et al. In vivo quantitative imaging of angiogenesis-targeted PFOB nanoparticles in a hypercholesterol rabbit model using 19F-MRI with ultra-short echo time balanced SSFP. *J Cardiovasc Magn Reson*. 2012;14(S1). doi:10.1186/1532-429X-14-S1-M8.
196. Hu L, Chen J, Yang X, et al. Rapid quantification of oxygen tension in blood flow with a fluorine nanoparticle reporter and a novel blood flow-enhanced-saturation-recovery sequence. *Magn Reson Med*. 2013;70(1):176–183. doi:10.1002/mrm.24436
197. Shimizu M, Kobayashi T, Morimoto H, et al. Tumor imaging with anti-CEA antibody labeled 19F emulsion. *Magn Reson Med*. 1987;5(3):290–295. doi:10.1002/mrm.1910050311
198. Thomas C, Counsell C, Wood P, et al. Use of fluorine-19 nuclear magnetic resonance spectroscopy and hydralazine for measuring dynamic changes in blood perfusion volume in tumors in mice. *J Natl Cancer Inst*. 1992;84(3):174–180. doi:10.1093/jnci/84.3.174
199. Mason RP, Shukla H, Antich PP. In vivo oxygen tension and temperature: simultaneous determination using 19F NMR spectroscopy of perfluorocarbon. *Magn Reson Med*. 1993;29(3):296–302. doi:10.1002/mrm.1910290304
200. Baldwin NJ, Wang Y, Ng TC. In situ 19F MRS measurement of RIF-1 tumor blood volume: corroboration by radioisotope-labeled [125I]-albumin and correlation to tumor size. *Magn Reson Imaging*. 1996;14(3):275–280. doi:10.1016/0730-725X(95)02080-D
201. Xu X, Yan Y, Liu F, et al. Folate receptor-targeted (19) F MR molecular imaging and proliferation evaluation of lung cancer. *J Magn Reson Imaging*. 2018;48(6):1617–1625. doi:10.1002/jmri.26177
202. Luo Z, Jin K, Pang Q, et al. On-demand drug release from dual-targeting small nanoparticles triggered by high-intensity focused ultrasound enhanced glioblastoma-targeting therapy. *ACS Appl Mater Interfaces*. 2017;9(37):31612–31625. doi:10.1021/acsami.7b10866
203. Liang X, Fang L, Li X, et al. Activatable near infrared dye conjugated hyaluronic acid based nanoparticles as a targeted theranostic agent for enhanced fluorescence/CT/photoacoustic imaging guided photothermal therapy. *Biomaterials*. 2017;132:72–84. doi:10.1016/j.biomaterials.2017.04.006
204. Wu L, Wen X, Wang X, et al. Local intratracheal delivery of perfluorocarbon nanoparticles to lung cancer demonstrated with magnetic resonance multimodal imaging. *Theranostics*. 2018;8(2):563–574. doi:10.7150/thno.21466